8 Fischer S, Spiegelhalder B, Eisenbarth J and Preussmann R: Investigations on the origin of tobacco-specific nitrosamines in mainstream smoke of cigarettes. Carcinogenesis *11*: 723-730, 1990.

9 Hecht SS, Hochalter JB, Villalta PW and Murphy SE: 2'-Hydroxylation of nicotine by cytochrome P450 2A6 and human liver microsomes: formation of a lung carcinogen precursor. Proc Natl Acad Sci USA *97*: 12493-12497, 2000.

10 Hecht SS and Hoffmann D: Tobacco-specific nitrosamines, an important group of carcinogens in tobacco and tobacco smoke. Carcinogenesis *9*: 875-884, 1988.

11 Ye YN, Liu ES, Shin VY, Wu WK and Cho CH: The modulating role of nuclear factor-kappaB in the action of alpha7-nicotinic acetylcholine receptor and cross-talk between 5-lipoxygenase and cyclooxygenase-2 in colon cancer growth induced by 4-(*N*-methyl-*N*-nitrosamino)-1-(3-pyridyl)-1-butanone. J Pharmacol Exp Ther *311*: 123-130, 2004.

12 Eaden JA, Abrams KR and Mayberry JF: The risk of colorectal cancer in ulcerative colitis: a meta-analysis. Gut *48*: 526-535, 2001.

13 van Hogezand RA, Eichhorn RF, Choudry A, Veenendaal RA and Lamers CB: Malignancies in inflammatory bowel disease: fact or fiction? Scand J Gastroenterol *Suppl*: 48-53, 2002.

14 Karban A and Eliakim R: Effect of smoking on inflammatory bowel disease: is it disease or organ specific? World J Gastroenterol *13*: 2150-2152, 2007.

15 Lakatos PL, Szamosi T and Lakatos L: Smoking in inflammatory bowel diseases: good, bad or ugly? World J Gastroenterol *13*: 6134-6139, 2007.

16 Eliakim R, Karmeli F, Rachmilewitz D, Cohen P and Fich A: Effect of chronic nicotine administration on trinitrobenzene sulphonic acid-induced colitis. Eur J Gastroenterol Hepatol *10*: 1013-1019, 1998.

17 Suzuki R, Miyamoto S, Yasui Y, Sugie S and Tanaka T: Global gene expression analysis of the mouse colonic mucosa treated with azoxymethane and dextran sodium sulfate. BMC Cancer *7*: 84, 2007.

18 Tanaka T, Kohno H, Suzuki R, Yamada Y, Sugie S and Mori H: A novel inflammation-related mouse colon carcinogenesis model induced by azoxymethane and dextran sodium sulfate. Cancer Sci *94*: 965-973, 2003.

19 Ward JM: Morphogenesis of chemically induced neoplasms of the colon and small intestine in rats. Lab Invest *30*: 505-513, 1974.

20 Nikitin AY, Alcaraz A, Anver MR, Bronson RT, Cardiff RD, Dixon D, Fraire AE, Gabrielson EW, Gunning WT, Haines DC, Kaufman MH, Linnoila RI, Maronpot RR, Rabson AS, Reddick RL, Rehm S, Rozengurt N, Schuller HM, Shmidt EN, Travis WD, Ward JM and Jacks T: Classification of proliferative pulmonary lesions of the mouse: recommendations of the Mouse Models of Human Cancers Consortium. Cancer Res *64*: 2307-2316, 2004.

21 Terry MB and Neugut AI: Cigarette smoking and the colorectal adenoma–carcinoma sequence: a hypothesis to explain the paradox. Am J Epidemiol *147*: 903-910, 1998.

22 Kohno H, Totsuka Y, Yasui Y, Suzuki R, Sugie S, Wakabayashi K and Tanaka T: Tumor-initiating potency of a novel heterocyclic amine, aminophenylnorharman in mouse colonic carcinogenesis model. Int J Cancer *121*: 506-513, 2007.

23 Hata K, Tanaka T, Kohno H, Suzuki R, Qiang SH, Kuno T, Hirose Y, Hara A and Mori H: Lack of enhancing effects of degraded lambda-carrageenan on the development of beta-catenin-accumulated crypts in male DBA/2J mice initiated with azoxymethane. Cancer Lett *238*: 69-75, 2006.

24 Miyamoto S, Suzuki R, Yasui Y, Kohno H, Sugie S, Murakami A, Ohigashi H and Tanaka T: Lack of enhancing effect of lauric acid on the development of aberrant crypt foci in male ICR mice treated with azoxymethane and dextran sodium sulfate. J Toxicol Pathol *20*: 93-100, 2007.

25 Yasui Y, Suzuki R, Miyamoto S, Tsukamoto T, Sugie S, Kohno H and Tanaka T: A lipophilic statin, pitavastatin, suppresses inflammation-associated mouse colon carcinogenesis. Int J Cancer *121*: 2331-2339, 2007.

26 Hecht SS, Kenney PM, Wang M, Trushin N, Agarwal S, Rao AV and Upadhyaya P: Evaluation of butylated hydroxyanisole, myo-inositol, curcumin, esculetin, resveratrol and lycopene as inhibitors of benzo[a]pyrene plus 4-(methylnitrosamino)-1-(3-pyridyl)-1-butanone-induced lung tumorigenesis in A/J mice. Cancer Lett *137*: 123-130, 1999.

27 Pereira MA, Tao LH, Wang W, Gunning WT and Lubet R: Chemoprevention: mouse colon and lung tumor bioassay and modulation of DNA methylation as a biomarker. Exp Lung Res *31*: 145-163, 2005.

28 Papanikolaou A, Wang QS, Delker DA and Rosenberg DW: Azoxymethane-induced colon tumors and aberrant crypt foci in mice of different genetic susceptibility. Cancer Lett *130*: 29-34, 1998.

29 Nilsson S, Carstensen JM and Pershagen G: Mortality among male and female smokers in Sweden: a 33 year follow-up. J Epidemiol Community Health *55*: 825-830, 2001.

30 Tsigris C, Chatzitheofylaktou A, Xiromeritis C, Nikiteas N and Yannopoulos A: Genetic association studies in digestive system malignancies. Anticancer Res *27*: 3577-3587, 2007.

31 Song P, Sekhon HS, Jia Y, Keller JA, Blusztajn JK, Mark GP and Spindel ER: Acetylcholine is synthesized by and acts as an autocrine growth factor for small cell lung carcinoma. Cancer Res *63*: 214-221, 2003.

32 Kim PM and Wells PG: Genoprotection by UDP-glucuronosyltransferases in peroxidase-dependent, reactive oxygen species-mediated micronucleus initiation by the carcinogens 4-(methylnitrosamino)-1-(3-pyridyl)-1-butanone and benzo[a]pyrene. Cancer Res *56*: 1526-1532, 1996.

33 Kosaka T, Miyata A, Ihara H, Hara S, Sugimoto T, Takedo O, Takahashi E and Tanabe T: Characterization of the human gene (*PTGS2*) encoding prostaglandin-endoperoxide synthase Eur J Biochem *221*: 889-897, 1994.

34 Wong HP, Yu L, Lam EK, Tai EK, Wu WK and Cho CH: Nicotine promotes cell proliferation *via* alpha7-nicotinic acetylcholine receptor and catecholamine-synthesizing enzymes-mediated pathway in human colon adenocarcinoma HT-29 cells. Toxicol Appl Pharmacol *221*: 261-267, 2007.

35 Liu ES, Ye YN, Shin VY, Yuen ST, Leung SY, Wong BC and Cho CH: Cigarette smoke exposure increases ulcerative colitis-associated colonic adenoma formation in mice. Carcinogenesis *24*: 1407-1413, 2003.

36 Kohno H, Suzuki R, Sugie S and Tanaka T: Suppression of colitis-related mouse colon carcinogenesis by a COX-2 inhibitor and PPAR ligands. BMC Cancer *5*: 46, 2005.

37 Liu ES, Ye YN, Shin VY, Wu WK, Wong BC and Cho CH: Interaction of cigarette smoking with cyclooxygenase-2 on ulcerative colitis-associated neoplasia in mice. Cancer Invest *25*: 750-757, 2007.

38 Chepiga TA, Morton MJ, Murphy PA, Avalos JT, Bombick BR, Doolittle DJ, Borgerding MF and Swauger JE: A comparison of the mainstream smoke chemistry and mutagenicity of a representative sample of the US cigarette market with two Kentucky reference cigarettes (K1R4F and K1R5F). Food Chem Toxicol *38*: 949-962, 2000.
39 Harris JE: Smoke yields of tobacco-specific nitrosamines in relation to FTC tar level and cigarette manufacturer: analysis of the Massachusetts Benchmark Study. Public Health Rep *116*: 336-343, 2001.
40 Kitajima S, Takuma S and Morimoto M: Tissue distribution of dextran sulfate sodium (DSS) in the acute phase of murine DSS-induced colitis. J Vet Med Sci *61*: 67-70, 1999.
41 Nishikawa A, Mori Y, Lee IS, Tanaka T and Hirose M: Cigarette smoking, metabolic activation and carcinogenesis. Curr Drug Metab *5*: 363-373, 2004.
42 Sohn OS, Fiala ES, Requeijo SP, Weisburger JH and Gonzalez FJ: Differential effects of CYP2E1 status on the metabolic activation of the colon carcinogens azoxymethane and methylazoxymethanol. Cancer Res *61*: 8435-8440, 2001.
43 Guengerich FP and Shimada T: Oxidation of toxic and carcinogenic chemicals by human cytochrome P-450 enzymes. Chem Res Toxicol *4*: 391-407, 1991.
44 Targan SR and Karp LC: Defects in mucosal immunity leading to ulcerative colitis. Immunol Rev *206*: 296-305, 2005.
45 Eliakim R and Karmeli F: Divergent effects of nicotine administration on cytokine levels in rat small bowel mucosa, colonic mucosa, and blood. Isr Med Assoc J *5*: 178-180, 2003.
46 Bonapace CR and Mays DA: The effect of mesalamine and nicotine in the treatment of inflammatory bowel disease. Ann Pharmacother *31*: 907-913, 1997.

Received February 28, 2008
Revised May 23, 2008
Accepted May 26, 2008

THE JOURNAL OF BIOLOGICAL CHEMISTRY VOL. 283, NO. 28, pp. 19864–19871, July 11, 2008

Stromal Fibroblasts Activated by Tumor Cells Promote Angiogenesis in Mouse Gastric Cancer*[S]

Received for publication, January 30, 2008, and in revised form, May 19, 2008 Published, JBC Papers in Press, May 21, 2008, DOI 10.1074/jbc.M800798200

Xiaoying Guo[‡§], Hiroko Oshima[‡], Takanori Kitmura[¶], Makoto M. Taketo[¶], and Masanobu Oshima[‡1]

From the [‡]Division of Genetics, Cancer Research Institute, Kanazawa University, Kanazawa 920-0934, Japan, the [§]Department of Occupational and Environmental Health, School of Public Health, China Medical University, Shenyang 110001, China, and the [¶]Department of Pharmacology, Kyoto University Graduate School of Medicine, Kyoto 606-8501, Japan

Myofibroblasts, also known as activated fibroblasts, constitute an important niche for tumor development through the promotion of angiogenesis. However, the mechanism of stromal fibroblast activation in tumor tissues has not been fully understood. A gastric cancer mouse model (*Gan* mice) was recently constructed by simultaneous activation of prostaglandin (PG) E_2 and Wnt signaling in the gastric mucosa. Because both the PGE_2 and Wnt pathways play a role in human gastric tumorigenesis, the *Gan* mouse model therefore recapitulates the molecular etiology of human gastric cancer. Microvessel density increased significantly in *Gan* mouse tumors. Moreover, the expression of vascular endothelial growth factor A (VEGFA) was predominantly induced in the stromal cells of gastric tumors. Immunohistochemistry suggested that VEGFA-expressing cells in the stroma were α-smooth muscle actin-positive myofibroblasts. Bone marrow transplantation experiments indicated that a subset of gastric myofibroblasts is derived from bone marrow. Importantly, the α-smooth muscle actin index in cultured fibroblasts increased significantly when stimulated with the conditioned medium of *Gan* mouse tumor cells, indicating that gastric tumor cells activate stromal fibroblasts. Furthermore, conditioned medium of *Gan* mouse tumor cells induced VEGFA expression both in embryonic and gastric fibroblasts, which further accelerated the tube formation of human umbilical vein endothelial cells *in vitro*. Notably, stimulation of fibroblasts with PGE_2 and/or Wnt1 did not induce VEGFA expression, thus suggesting that factors secondarily induced by PGE_2 and Wnt signaling in the tumor cells are responsible for activation of stromal fibroblasts. Such tumor cell-derived factors may therefore be an effective target for chemoprevention against gastric cancer.

Accumulating evidence has indicated that cancer development is regulated by interactions between tumor cells and activated stromal cells (1). Experiments in mouse models have shown that fibroblasts in the stromal microenvironment play an important role in tumor formation (2–4). Moreover, carcinoma-associated fibroblasts (CAFs)[2] stimulate tumor progression of the initiated epithelial cells (5). Stromal fibroblasts isolated from human breast cancer show distinctive gene expression profiles, although no genetic alteration is found (6). These results indicate that the stromal fibroblasts in tumor tissues possess biological characteristics distinct from those of the normal fibroblasts, which contribute to tumor development. Immunohistochemical studies have shown that a large number of myofibroblasts, which express α-smooth muscle actin (α-SMA), are present in the stromal component of human breast cancer, intestinal polyps, and gastric cancer (7–9). These myofibroblasts, which are also known as "activated fibroblasts," therefore contribute to tumor formation.

The promotion of angiogenesis is an important function of myofibroblasts during tumorigenesis. Angiogenesis is a key mechanism that supports tumor development by providing nutrients and oxygen (10). The CAFs extracted from human breast cancer, which exhibit the traits of myofibroblasts, promote angiogenesis through the expression of stromal cell-derived factor 1 (11). Moreover, prostaglandin E_2 (PGE_2) stimulates intestinal myofibroblasts to express vascular endothelial growth factor A (VEGFA), epidermal growth factor-like growth factor, and amphiregulin, thus leading to the promotion of angiogenesis as well as epithelial proliferation (12). In addition, stromal cell-derived PGE_2 plays an important role in angiogenesis in intestinal tumorigenesis through the induction of VEGF and basic fibroblast growth factor (13, 14). Although it has been shown that the conversion of fibroblasts constitutes the major source of myofibroblasts (15), the mechanisms underlying stromal activation and promotion of angiogenesis are still not fully understood. It is important to examine the *in vivo* tumor mouse model to understand the interaction between tumor cells, stromal fibroblasts, and angiogenesis.

* This work was supported by grants from the Ministry of Education, Culture, Sports, Science and Technology of Japan, the Ministry of Health, Labour and Welfare of Japan, and Takeda Science Foundation, Japan. The costs of publication of this article were defrayed in part by the payment of page charges. This article must therefore be hereby marked "*advertisement*" in accordance with 18 U.S.C. Section 1734 solely to indicate this fact.

[S] The on-line version of this article (available at http://www.jbc.org) contains supplemental Figs. 1–3.

[1] To whom correspondence should be addressed: Division of Genetics, Cancer Research Institute, Kanazawa University, 13-1 Takara-machi, Kanazawa 920-0934, Japan. Tel.: 81-76-265-2721; Fax: 81-76-234-4519; E-mail: oshimam@kenroku.kanazawa-u.ac.jp.

[2] The abbreviations used are: CAF, carcinoma-associated fibroblast; α-SMA, α-smooth muscle actin; CM, conditioned medium; COX-2, cyclooxygenase-2; GF, gastric fibroblasts; HGF, hepatocyte growth factor; HUVEC, Human umbilical vein endothelial cell; LMD, laser microdissection; MEF, mouse embryonic fibroblast; mPGES-1, microsomal prostaglandin E synthase-1; MVD, microvessel density; PGE_2, prostaglandin E_2; RT, reverse transcription; TNF-α, tumor necrosis factor-α; VEGFA, vascular endothelial growth factor-A; vWF, vonWillebrand factor; ELISA, enzyme-linked immunosorbent assay; IL, interleukin; GFP, green fluorescent protein; EGFP, enhanced GFP; GM-CSF, granulocyte-macrophage colony-stimulating factor; DMEM, Dulbecco's modified Eagle's medium.

A gastric cancer mouse model (*K19-Wnt1/C2mE* mice) was recently established by the transgenic expression of Wnt1, cyclooxygenase-2 (COX-2), and microsomal PGE synthase-1 (mPGES-1) in the gastric mucosa (16). COX-2, a rate-limiting enzyme for prostaglandin biosynthesis, is induced in more than 70% of gastric cancer and plays an important role in gastric tumorigenesis (17). An inducible PGE_2-converting enzyme, mPGES-1, appears to be functionally coupled with COX-2 (18), and mPGES-1 expression is also induced in gastric cancer, thus suggesting an increased PGE_2 level in gastric cancer tissues (19). On the other hand, the canonical Wnt signaling is a critical pathway for gastrointestinal tumorigenesis (20). β-Catenin nuclear localization, a hallmark of Wnt pathway activation, is found in 29% of gastric cancer (21), suggesting that the activation of the Wnt pathway is one of the major causes for gastric carcinogenesis. Importantly, *K19-Wnt1/C2mE* mice, in which both the PGE_2 and Wnt pathways are activated simultaneously, develop intestinal-type gastric adenocarcinomas (16). Therefore, *K19-Wnt1/C2mE* mice (hereafter *Gan* mice for Gastric neoplasia) recapitulate a subpopulation of human gastric cancers not only in molecular mechanism but also in tumor pathology.

This study examined the epithelial-stromal interaction in tumor angiogenesis using the *Gan* mouse model. Although it has been established that PGE_2 signaling is important for angiogenesis in intestinal tumors (12–14, 22), the mechanisms underlying the induction of angiogenic factors remain to be elucidated. We show that *Gan* mouse gastric tumor cells activate stromal fibroblasts to become myofibroblasts, and that these myofibroblasts stimulated by gastric tumor cells express VEGFA and other angiogenic factors, which may lead to the promotion of angiogenesis.

EXPERIMENTAL PROCEDURES

Transgenic Mice—The establishment of the *K19-C2mE*, *K19-Wnt1*, and *Gan* mice (*K19-Wnt1/C2mE*) has been described previously (16, 23). Briefly, COX-2 and mPGES-1 are expressed in the stomach of *K19-C2mE* mice, whereas Wnt1 is expressed in the stomach of *K19-Wnt1* mice. The expression of these genes is regulated by the cytokeratin 19 gene promoter. For the inhibition of COX-2, *Gan* mice from 28 to 30 weeks of age were injected subcutaneously with 10 mg/kg/day of NS-398 (Sigma) for 3 weeks ($n = 3$). All animal experiments were carried out according to the protocol approved by the Committee on Animal Experimentation of Kanazawa University.

Histology and Immunohistochemistry—Mouse stomach tissues were fixed in 4% paraformaldehyde, paraffin-embedded, and sectioned at 4-μm thickness. These sections were stained with hematoxylin and eosin and processed for immunostaining. To detect capillary vessels, polyclonal anti-von Willebrand factor (vWF) antibody was used (DakoCytomation, Carpinteria, CA) as the primary antibody of immunohistochemistry. To detect VEGFA-expressing cells, monoclonal anti-VEGF antibody (Santa Cruz Biotechnology, Santa Cruz, CA) was used. To detect lymphatic vessels, polyclonal anti-Lyve-1 antibody (Acris Antibodies, Hiddenhausen, Germany) was used. To detect macrophages, rat monoclonal antibody for F4/80 (Serotec, Oxford, UK) was used. To detect myofibroblasts, polyclonal anti-α-smooth muscle actin (Sigma) and monoclonal anti-tenascin-c antibodies (Abcam) were used. To detect smooth muscle cells, anti-calponin-1 monoclonal antibody (Epitomics) was used. To detect GFP, polyclonal anti-GFP antibody (Molecular Probes) was used. The MOM kit (Vector Laboratories, Burlingame, CA) was used to minimize the background. Staining signals were then visualized using the Vectorstain Elite kit (Vector Laboratories). For immunofluorescence, Alexa Fluor 594 or Alexa Fluor 488 antibody (Molecular Probes, Eugene, OR) was used as the secondary antibody.

Immunocytochemistry—Mouse embryonic fibroblasts (MEFs) and gastric fibroblasts (GFs) grown on coverslips were fixed with 10% neutral buffered formalin and permeabilized with 0.1% Triton X-100 in phosphate-buffered saline. Anti-α-SMA monoclonal antibody (Sigma) was used as the primary antibody, and anti-mouse IgG Alexa Fluor 488 (Molecular Probes) was used as the secondary antibody. Next, the coverslips were mounted using Vectashield mounting medium (Vector Laboratories) that contained 4′,6-diamidino-2-phenylindole for nuclear staining. The number of α-SMA-positive cells was counted using five microscopic fields for each sample, and the mean α-SMA positive index was calculated.

Scoring Microvessel Density—Microvessel density (MVD) was scored using histological sections immunostained with anti-vWF antibody. The number of vessels was then counted in high magnification fields (×400) for each group ($n = 3$). At least five microscopic fields per mouse were scored for each genotype, and then the mean relative MVD to the wild-type MVD was calculated.

Reverse Transcription (RT)-PCR—Total RNA was extracted from the tissues or cells using ISOGEN (Nippon Gene, Tokyo, Japan). Epithelial and stromal tissues were isolated from cryosections, respectively, using a laser microdissection (LMD) system (Leica Microsystems, Wetzler, Germany). Extracted RNA was reverse-transcribed and PCR-amplified by GeneAmp PCR System 9700 (Applied Biosystems). RT-PCR was carried out using the following primer set: VEGFA (F-5′-CTTCCTACAGCACAGCAGATGTGAA-3′; R-5′-TGGTGACATGGTTAATCGGTCTTTC-3′) and hepatocyte growth factor (HGF) (F-5′-TTCCCAGCTGGTCTATGGTC-3′; R-5′-TGGTGCTGACTGCATTTCTC-3′). Specific β-actin primers were used as an internal control. For real time RT-PCR, total RNA was reverse-transcribed using the PrimeScript RT reagent kit (Takara, Japan), and then it was PCR-amplified by ABI Prism 7900HT (Applied Biosystems) using SYBR Premix Ex TaqII (Takara, Japan). The primer sets used in real time RT-PCR to detect VEGFA, HGF, Tie2, and CXCR4 were purchased (Takara, Japan).

Bone Marrow Transplantation—Bone marrow cells were isolated from EGFP transgenic mice (24). Bone marrow cells were suspended in phosphate-buffered saline at 1×10^7 cells. The 6-week-old recipient *K19-C2mE* mice and wild-type mice were irradiated with 8 Gy γ-ray and transplanted with 1×10^6 GFP+ donor cells intravenously. *K19-C2mE* mice that received a bone marrow transplant were autopsied 20 weeks later.

Cell Culture Experiments—MEFs were prepared from 12.5 days post-coitum embryos and cultured with DMEM (Invitrogen) containing 10% fetal bovine serum. Human umbilical vein

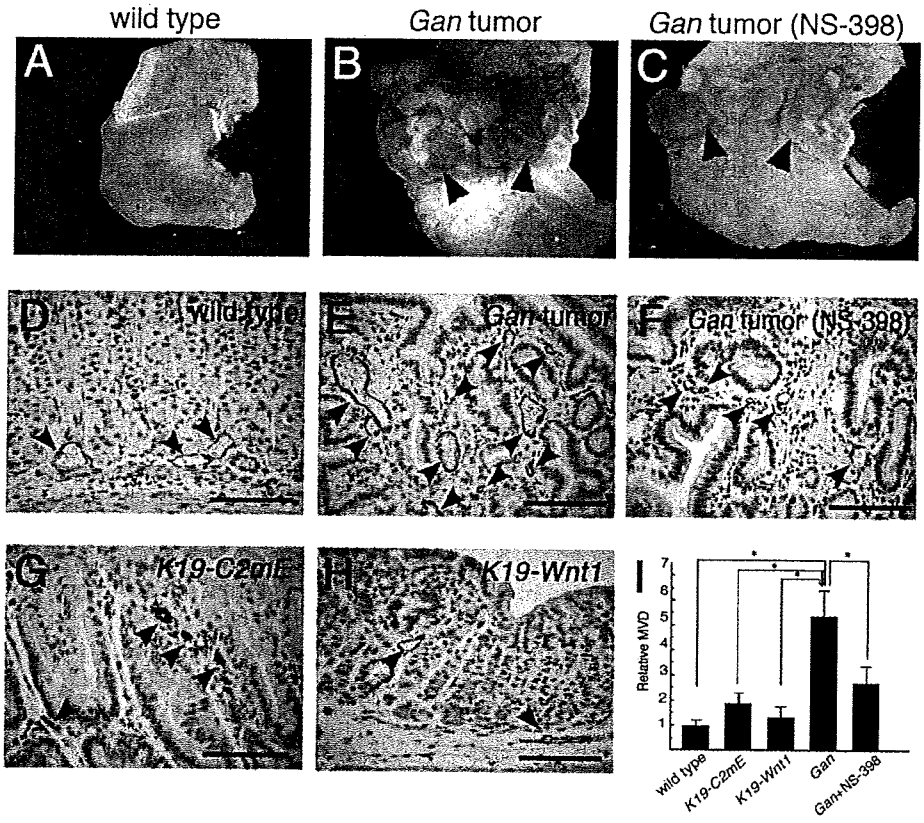

FIGURE 1. **Promotion of angiogenesis in *Gan* mouse gastric tumors.** *A–C*, representative macroscopic photographs of the stomach of wild-type mouse (*A*), *Gan* mouse (*B*), and NS-398-treated *Gan* mouse (*C*). *Arrowheads* in *B* and *C* indicate gastric tumors of *Gan* mice. Note that NS-398 treatment suppressed hypermia of gastric tumors. *D–H*, immunostaining for capillary vessels using anti-vWF antibody in the gastric mucosa of wild-type stomach (*D*), *Gan* mouse tumor (*E*), NS-398-treated *Gan* mouse tumor (*F*), *K19-C2mE* stomach (*G*), and *K19-Wnt1* stomach (*H*). The *arrowheads* indicate vWF-positive capillary vessels. *Bars* indicate 50 μm. *I*, relative MVD in the respective genotypes to the wild-type level (mean ± S.D.). *, $p < 0.05$.

endothelial cells (HUVECs) were purchased from American Type Culture Collection and maintained using the EGM-2 bullet kit (Lonza, Basel, Switzerland). The primary gastric epithelial cells were prepared as described previously (23) and cultured on collagen-coated 6-well plates. When the cell density reached 80% confluence, the medium was replaced with DMEM/F-12, and the conditioned medium was collected after a culture of 48 h. For the isolation of GFs, mouse stomach tissues or gastric tumors were digested with collagenase (1 mg/ml at 37 °C for 30 min), washed with DMEM, seeded in collagen-coating dishes, and washed with medium after 30 min to remove epithelial cells. After two rounds of passages, epithelial cells were absent in the culture, and fast growing GFs were enriched. For direct co-culture experiments, gastric epithelial cells and MEFs were mixed at a ratio of 1:1 and plated in 6-well plates. For indirect co-culture experiments, 1×10^5 MEFs or GFs were plated in 48-well plates, and the medium was replaced with mixture of conditioned medium from the primary culture (250 μl) and fresh DMEM (250 μl). At 48 h after stimulation with conditioned medium, medium and cell lysates were collected and used for the following assays. To analyze VEGFA induction by cytokines, MEFs were stimulated with IL-1α, IL-6, IL-17α, GM-CSF (R & D Systems) or tumor necrosis factor (TNF)α (Calbiochem) at 10 and 100 ng/ml for 24 h, and the VEGFA expression in the medium was examined by ELISA.

Cytokine Expression Analysis—Conditioned media obtained from the primary cultured *Gan* mouse tumor cells and wild-type mouse gastric epithelial cells were used for the expression analysis of cytokines. Expression of IL-1α, IL-1β, IL-2, IL-4, IL-6, IL-10, IL-12, IL-17α, interferon-γ, TNF-α, granulocyte-CSF, and GM-CSF in each medium was examined using the Multi-Analyte Profiler ELISArray kit (Super Array) according to the manufacturer's protocol.

ELISA—The concentration of VEGFA in the culture medium was measured using an ELISA kit (BioSource International, Camarillo, CA), and the total protein of cultured cells was measured using a BCA protein detection kit. For the primary culture of epithelial cells, VEGFA concentration was calculated as medium VEGFA (pg) per total protein (mg) of cells or medium volume (ml) because of difficulty in counting the number of cells. For the MEF culture, medium VEGFA (pg) per 10^5 cells was calculated.

HUVEC Tube Formation Assay—HUVECs (5×10^4 cells) were suspended in mixture of conditioned medium (125 μl) and EGM-2 medium (125 μl) in the presence or absence of PGE_2 at 1 μM with 0.5% fetal bovine serum, and seeded on 150 μl of Matrigel in 48-well culture plates. After incubation for 18–24 h, photographs of each well were taken, and the number of tubular structures and the length of the tubes in each field were measured using Image J application software (National Institutes of Health).

Statistical Analysis—Statistical analyses were carried out by Student's *t* test, and *p* values <0.05 were considered to be statistically significant.

RESULTS

Gan mice (*K19-Wnt1/C2mE* mice) develop gastric adenocarcinomas in the glandular stomach caused by the simultaneous activation of Wnt and PGE_2 pathways (16). Notably, gastric tumors developed in *Gan* mice showed hyperemia that was not found in the wild-type mouse stomach (Fig. 1, *A* and *B*). Histologically, numerous capillary vessels were detected in the *Gan* mouse gastric tumors by immunostaining using anti-vWF antibody, whereas vessels were sparsely found in the normal gastric mucosa (Fig. 1, *D* and *E*). The MVD in the *Gan* mouse tumors increased significantly to more than five times that of the wild-type level (Fig. 1*I*). PGE_2 signaling plays an important role in

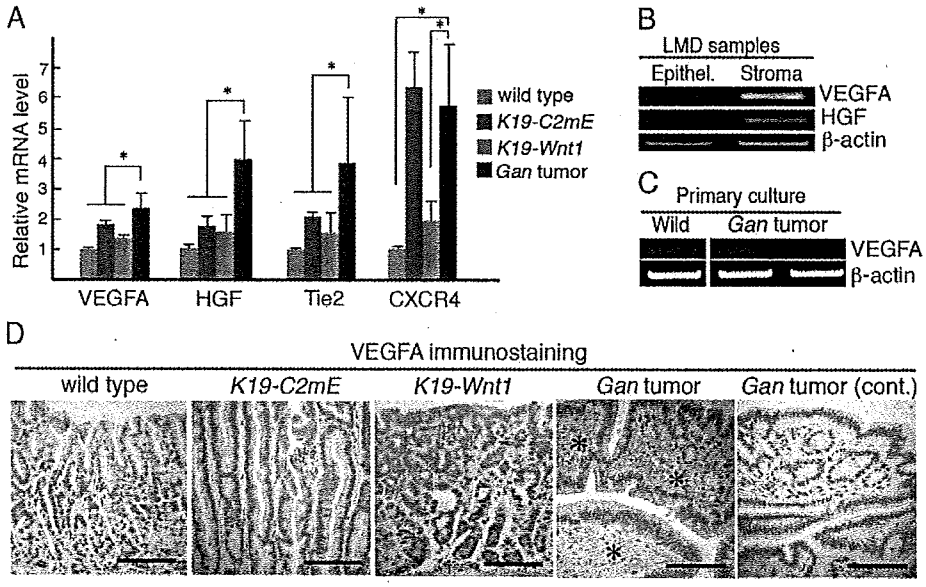

FIGURE 2. **Expression of VEGF in the stroma of *Gan* mouse gastric tumors.** *A*, real time RT-PCR results for VEGF, HGF, Tie2, and CXCR4 in gastric mucosa of the wild-type, *K19-C2mE*, and *K19-Wnt1* mice and in *Gan* mouse tumors. The calculated relative mRNA levels to the wild-type level are shown (mean ± S.D.). *, $p < 0.05$. *B*, representative RT-PCR for VEGFA and HGF in the epithelium and stroma of *Gan* mouse tumors isolated using an LMD system. *C*, representative RT-PCR for VEGFA in the primary cultured epithelial cells from the wild-type mouse stomach and *Gan* mouse tumors. *D*, immunostaining for VEGFA in the gastric mucosa of wild-type, *K19-C2mE*, and *K19-Wnt1* mice and *Gan* mouse tumor (from *left* to *right*). The *asterisks* indicate the VEGFA-expressing stromal cells (*brown*) located in the *Gan* mouse gastric tumors. Immunostaining specificity was confirmed by negative control staining of nonprimary antibody using a *Gan* tumor section (*cont*, control).

angiogenesis in intestinal tumorigenesis (12–14, 22). The treatment of *Gan* mice with NS-398, a COX-2 inhibitor, resulted in suppression of hyperemia of gastric tumors (Fig. 1*C*) caused by a decreased number of capillary vessels in the gastric tumors (Fig. 1, *F* and *I*). These results indicate that the activation of COX-2/PGE_2 signaling is important for angiogenesis in gastric cancer. On the other hand, the number of capillary vessels and MVD did not increase in the gastric mucosa of *K19-C2mE* mice or *K19-Wnt1* mice (Fig. 1, *G–I*), which express PGE_2 or Wnt1 in the stomach, respectively (16, 23). Accordingly, it is possible that the activation of both the PGE_2 and Wnt pathways are important for angiogenesis in gastric tumors. However, further experiments demonstrated that secondarily induced factors in the tumor cells are responsible for angiogenesis (see below and see Fig. 4, *C* and *D*), although activation of both PGE_2 and Wnt pathways is essential for gastrointestinal tumorigenesis (16, 25).

The COX-2 pathway is also important for lymphangiogenesis (26). However, lymphatic vessels were rarely detected in the gastric mucosa of the wild-type, *K19-C2mE*, and *K19-Wnt1* mice as well as *Gan* mouse gastric tumors (supplemental Fig. 1). In the stomach of these mouse models, lymphatic vessels were predominantly found in the smooth muscle layers. Accordingly, it is conceivable that activation of PGE_2 and Wnt signaling does not promote lymphangiogenesis in gastric cancer.

Consistent with the results of the MVD analyses, the VEGFA mRNA level determined by real time RT-PCR significantly increased in the *Gan* mouse gastric tumors in comparison with that in the wild-type, *K19-C2mE*, or *K19-Wnt1* mouse stomach (Fig. 2*A*). We also examined expression of HGF, Tie2, and CXCR4 by real time RT-PCR, because they have been reported to play a role in angiogenesis (27–29). Interestingly, the expression of all these genes significantly increased in the *Gan* mouse tumors in comparison with that in the gastric mucosa of other genotype mice except CXCR4 in *K19-C2mE* mice (Fig. 2*A*). The expression of CXCR4 is induced in both *K19-C2mE* and Gan mice, thus suggesting the PGE_2-dependent induction. These results indicate that several angiogenic pathways are activated simultaneously in the gastric tumor tissues, although the underlying molecular mechanisms remain to be investigated. Next, epithelial cells and stromal cells were isolated from *Gan* gastric tumor specimens using the LMD system. The expression of VEGFA and HGF was predominantly detected in the stromal cells but not in the epithelial cells (Fig. 2*B*). Consistently, VEGFA mRNA was at the wild-type level in the primary cultured *Gan* tumor epithelial cells, in which stromal cells were removed (Fig. 2*C*). These results indicate that stromal cells are the major source for VEGFA and HGF in gastric tumors. Further analyses focused on the expression of VEGFA because of its significant role in angiogenesis. We confirmed the abundant expression of VEGFA in the stromal cells of *Gan* mouse gastric tumors by immunostaining (Fig. 2*D*, *asterisks*). In contrast, VEGFA-expressing cells were rarely found in the stroma of the wild-type, *K19-C2mE*, or *K19-Wnt1* mouse gastric mucosa. We confirmed the immunostaining specificity by a negative control of nonprimary antibody using a *Gan* tumor tissue section (Fig. 2*D*, *right*).

It has been shown that myofibroblasts play a key role in tumor angiogenesis (9, 10). Therefore, the expression of α-SMA was examined in the *Gan* mouse tumors, which was a defining characteristic of the myofibroblasts (30). Importantly, a substantial number of α-SMA-positive cells were found in *Gan* mouse tumor stroma, whereas α-SMA-positive cells were sparsely detected in the nontumorous gastric mucosa (Fig. 3*A*). Moreover, most α-SMA-positive cells expressed tenascin-c, another marker for myofibroblasts (Fig. 3*B*, *left*). In contrast, the majority of α-SMA-positive cells were negative for smooth muscle specific marker calponin-1, although small number of cells expressed both α-SMA and calponin-1 (Fig. 3*B*, *right*). These results strongly suggest the major cell type expressing VEGFA in the *Gan* mouse tumor stroma are myofibroblasts (compare Fig. 2*D* and Fig. 3*A*). On the other hand, immunostaining analyses revealed that VEGFA expression was rarely found in the macrophages or capillary vessels in the *Gan* mouse tumors (Fig. 3*C*).

It has been reported that bone marrow cells contribute to stromal myofibroblasts of tumor tissues (31). Moreover, inflammatory responses significantly increase the contribution

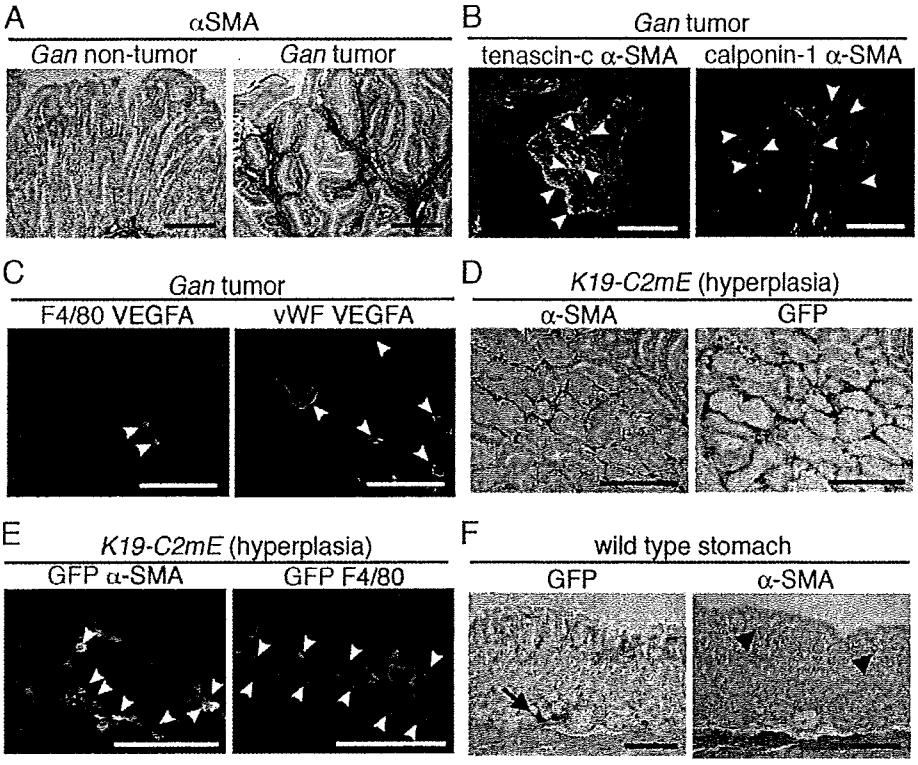

FIGURE 3. **Bone marrow-derived myofibroblasts in gastric lesions.** *A*, immunostaining for α-SMA-expressing cells (*brown*) in nontumorous (*left*) and tumor region (*right*) of *Gan* mouse stomach. *B*, double immunostaining for tenascin-c (*green*) and α-SMA (*red*), and calponin-1 (*green*) and α-SMA (*red*). The *arrowheads* indicate tenascin-c and α-SMA double-positive cells (*left*), and calponin-1-negative and α-SMA-positive cells (*right*). *C*, double immunostaining for F4/80 (*green*) and VEGFA (*red*), and vWF (*green*) and VEGFA (*red*). The *arrowheads* indicate macrophages (*left*) and capillary vessels (*right*). *D*, immunostaining for α-SMA (*left*) and GFP (*right*) in gastric hyperplasia of *K19-C2mE* mice that received a bone marrow transplantation from EGFP transgenic mice. *E*, double immunostaining for GFP (*green*) and α-SMA (*red*), and GFP (*green*) and F4/80 (*red*) in gastric hyperplasia of *K19-C2mE* mice that received a bone marrow transplantation from EGFP transgenic mice. The *arrowheads* indicate double-positive cells for GFP and α-SMA (*left*) and GFP and F4/80 (*right*). *F*, immunostaining for GFP (*left*) and α-SMA (*right*) in the normal gastric mucosa of a wild-type mouse that received a bone marrow transplant from EGFP transgenic mice. The *arrow* indicates infiltrated bone marrow-derived mononuclear cells. The *arrowheads* indicate the α-SMA-positive pericytes of capillary vessels. *Bars* in *A–F* indicate 100 μm.

of bone marrow cells to myofibroblasts (32). Therefore, the contribution of bone marrow cells to gastric myofibroblasts was examined using the *K19-C2mE* mice that develop inflammation-associated gastric hyperplasia caused by increased PGE_2 signaling (23). As in the *Gan* mouse tumor tissues, α-SMA-positive cells were increased in the stroma of *K19-C2mE* mouse stomach (Fig. 3*D*, *left*). Bone marrow transplantation to γ-ray irradiated *K19-C2mE* mice from EGFP transgenic mice revealed that the number of GFP-positive bone marrow-derived cells infiltrated to the gastric stroma (Fig. 3*D*, *right*). Notably, the subset of α-SMA-positive cells in the gastric stroma also showed GFP expression (Fig. 3*E*, *left*). The mean percentage of GFP-positive cells in the α-SMA-expressing cells was 12.1%, thus indicating that part of the stromal myofibroblasts is derived from bone marrow cells. We also found 58% of the GFP-positive cells in the gastric stroma to be macrophages (Fig. 3*E*, *right*). In contrast, bone marrow cells rarely contributed to normal gastric mucosa of the transplanted wild-type mice except with infiltrated mononuclear cells (Fig. 3*F*).

To examine the activation of stromal cells by tumor cells, MEFs and gastric fibroblasts (GFs) were treated with a conditioned medium (CM) of the primary cultured *Gan* tumor epithelial cells (supplemental Fig. 2). Importantly, the α-SMA index increased significantly in both MEFs and GFs when treated with *Gan* tumor CM. These results suggest that tumor epithelial cells activate stromal fibroblasts, thus resulting in conversion to myofibroblasts. It is thus conceivable that both bone marrow cells and preexisting fibroblasts therefore contribute to gastric myofibroblasts.

We next examined whether gastric tumor epithelial cells induce VEGFA expression in stromal fibroblasts. We performed direct or indirect co-culture experiments using the primary cultures of gastric epithelial cells and fibroblasts (Fig. 4*A*). MEFs as well as GFs were used for the experiments, because MEFs were activated by CM of *Gan* tumor cells (supplemental Fig. 2). In the direct co-culture of MEFs and *Gan* tumor cells, the VEGFA mRNA level increased significantly in comparison with that in either of MEF or tumor epithelial cell monoculture (Fig. 4*B*, *left*). Consistently, the VEGFA concentration in the media increased more than 10-fold in the direct co-culture of MEFs and *Gan* tumor cells than that in either monoculture. Interestingly, VEGFA mRNA level also increased in the direct co-culture of MEFs and wild-type epithelial cells (Fig. 4*B*, *right*), suggesting that factor(s) inducing VEGFA are also expressed in the cultured normal epithelial cells at a basal level. However, VEGFA concentration in the medium was significantly higher in the co-culture of MEFs with *Gan* tumor cells (14,100 pg/ml) in comparison with that with normal gastric epithelial cells (5,200 pg/ml). We confirmed by real time RT-PCR that the VEGFA expression level increased in the co-culture of *Gan* tumor epithelial cells and MEFs. These results suggest that fibroblast-stimulating factors for VEGFA expression are significantly induced in the gastric tumor epithelial cells.

We next examined the VEGFA induction in MEFs by indirect co-culture experiments. Conditioned media of the primary cultured epithelial cells were prepared from the wild-type, *K19-C2mE*, and *K19-Wnt1* mouse stomach and *Gan* mouse tumors. Before the experiments, the VEGFA concentration in the respective CM was confirmed to be at the same basal level (supplemental Fig. 3). The treatment of MEFs with CM of the wild-type epithelial cells resulted in increased VEGFA expression, which may be caused by activating factors nonspecifically expressed in the cultured normal epithelial cells, therefore con-

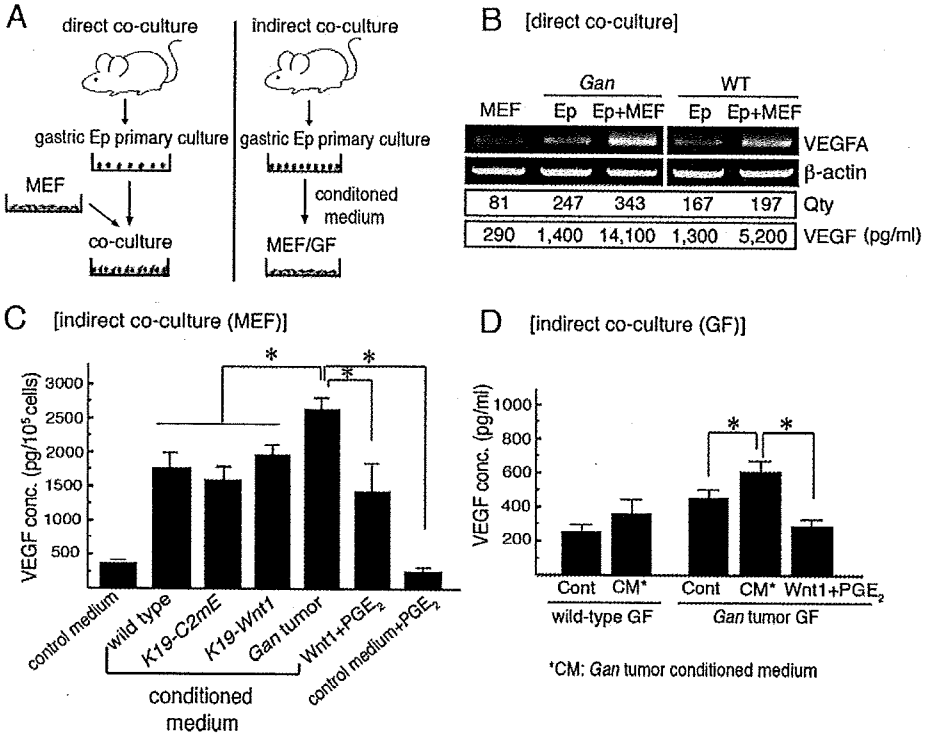

FIGURE 4. **The induction of VEGFA in fibroblasts stimulated with gastric tumor epithelial cells.** *A*, schematic diagram of the direct and indirect co-culture experimental methods, respectively. *Ep* indicates epithelial cells. *B*, representative RT-PCR results for VEGF expression in the direct co-culture (*Ep+MEF*) and monoculture (*MEF* or *Ep*). *Gan* indicates the tumor epithelial cells isolated from *Gan* mice (*left*), whereas *WT* indicates wild-type mouse gastric epithelial cells (*right*). β-Actin was used as an internal control. Quantity values (*Qty*) of independently performed real time RT-PCR for the respective culture conditions are indicated *below* the panel. The concentration of VEGF (pg/ml) in the medium measured by ELISA is also shown *below* the panel. *C*, VEGF concentration in the MEF culture medium is shown (mean ± S.D.). MEFs were stimulated with CM of wild-type, *K19-C2mE*, and *K19-Wnt1* mouse gastric epithelial cells and *Gan* mouse tumor cells. *Control medium* did not contain CM of epithelia. *Wnt1+PGE*$_2$ indicates CM of *K19-Wnt1* epithelial cell culture supplemented with PGE_2 at 1 μM. *, $p < 0.05$. Note that the VEGF level increased significantly beyond the wild-type level in MEFs stimulated with CM of *Gan* tumor cells. *D*, VEGF concentration in the GF culture medium is shown (mean ± S.D.). GFs derived from wild-type mouse stomach (*left*) or *Gan* mouse tumors (*right*) were treated with CM of *Gan* mouse tumor cells (*CM*), wild-type mouse gastric epithelial cells (*Cont*), or *K19-Wnt1* epithelial cells supplemented with PGE_2 at 1 μM (*Wnt1+PGE*$_2$). *, $p < 0.05$.

sidered as background (Fig. 4*C*). The VEGFA expression level of MEFs treated with CM of the *K19-C2mE* or *K19-Wnt1* epithelial cells was also at the background level, thus suggesting that either PGE_2 or Wnt signaling alone cannot induce VEGFA in the fibroblasts. Consistently, treatment of MEFs with PGE_2 alone resulted in no increase of the VEGFA level in the medium. In contrast, CM of *Gan* tumor cells increased VEGFA expression significantly beyond the background level (Fig. 4*C*), indicating that *Gan* tumor cells express soluble factors that induce VEGFA in fibroblasts. Importantly, however, the VEGFA level was not increased when MEFs were stimulated with CM of *K19-Wnt1* cells supplemented with PGE_2, which contained both PGE_2 and Wnt1 (Fig. 4*C*). These results rule out the possibility that direct stimulation by PGE_2 and Wnt ligand induces VEGFA expression in fibroblasts. Therefore, it is conceivable that secondary factors induced by PGE_2 and Wnt signaling in the tumor cells stimulate fibroblasts, although both the PGE_2 and Wnt pathways are required for tumor formation (16).

We next tested whether gastric tumor cells also stimulate GFs to express VEGFA. Notably, treatment of *Gan* tumor GFs with CM of the tumor epithelial cells significantly increased the VEGFA concentration in the medium (Fig. 4*D*). Consistent with the results in MEF experiments (Fig. 4*C*), the CM of *K19-Wnt1* cells supplemented with PGE_2 did not increase the VEGFA level in *Gan* tumor GFs, thus indicating that factor(s) other than Wnt and PGE_2 are responsible for the VEGFA induction in GFs. Although VEGFA in the wild-type GFs also increased after treatment with CM, the increase was not significant. Accordingly it is possible that gastric tumor fibroblasts possess higher responsiveness to stimulation by the tumor cells than normal stomach fibroblasts.

Inflammatory responses are associated with the development of gastric hyperplasia in the *K19-C2mE* mice (23). We thus examined whether tumor cell-derived cytokines play a role in VEGFA induction in fibroblasts. Cytokine ELISAs revealed the level of IL-1α, IL-6, IL-17α, G-CSF, and GM-CSF in the medium of *Gan* tumor cell cultures to increase significantly in comparison with that in the wild-type epithelial cells (Fig. 5). However, the treatment of MEFs with IL-1α, IL-6, IL-17α, GM-CSF as well as TNF-α did not induce VEGFA expression, whereas the CM of *Gan* mouse tumor cells did (data not shown and Fig. 4*C*). These results suggest that other factors than inflammatory cytokines expressed by tumor cells play a role in the VEGFA induction in stromal fibroblasts.

We finally examined whether fibroblasts activated by tumor cells induce angiogenesis *in vitro* using the HUVEC tube formation assay. Secondary CM was prepared from MEF cultures after stimulation with CM of wild-type or gastric tumor epithelial cells. HUVECs formed a network of capillary-like structures after 18 h of culture in Matrigel (Fig. 6*A*, *left*). Significantly, CM of MEFs stimulated with *Gan* tumor cells dramatically accelerated tube formation (Fig. 6*A*, *right*), in comparison with those treated with CM of MEFs treated with wild-type epithelium (Fig. 6*A*, *center*). The number and length of HUVEC tubes increased by 14 and 10 times, respectively, by treatment with CM of tumor cell-stimulated MEFs (Fig. 6, *B* and *C*). Consistent with the results of co-culture experiments (Fig. 4, *C* and *D*), CM of MEFs stimulated with CM of *K19-Wnt1* gastric epithelial cells with PGE_2 did not increase HUVEC tube formation (Fig. 6, *B* and *C*). Although the VEGF level increased in the culture medium of MEFs stimulated with CM of wild-type or *K19-Wnt1* mouse epithelium (Fig. 5*C*), HUVEC tube formation was enhanced significantly by CM of MEFs treated with *Gan* mouse

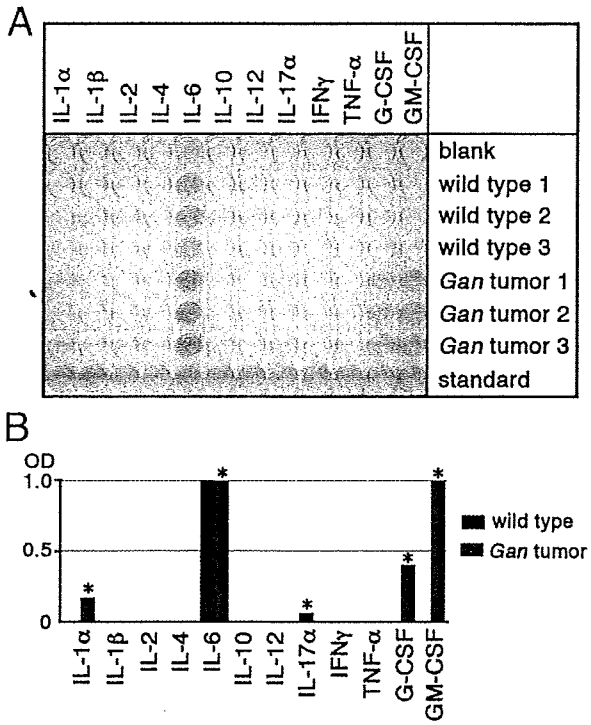

FIGURE 5. **Expression of inflammatory cytokines from the primary cultured gastric tumor epithelial cells.** *A*, photograph of a representative ELISA plate. Three independent culture medium samples each for wild-type gastric epithelial cells and *Gan* tumor epithelial cells were used. A *yellow* color indicates positive reaction. *B*, mean OD values of ELISA results for indicated cytokines are shown. *OD* >1.0 is indicated as 1.0. *, $p < 0.05$ *versus* wild-type level.

tumor cells in comparison with that of wild-type cells or *K19-Wnt1* epithelial cells with PGE_2. These results, taken together, suggest that gastric tumor cells activate fibroblasts to promote angiogenesis through the induction of not only VEGFA but also other angiogenic factors as shown in Fig. 2*A*.

DISCUSSION

We have previously shown using genetic mouse models that the COX-2/PGE_2 pathway is important for angiogenesis in intestinal polyps (13, 14). The disruption of the COX-2 gene (*Ptgs2*) or PGE_2 receptor EP2 gene (*Ptger2*) causes suppression of VEGF expression and decrease of MVD in tumor tissues. On the other hand, the VEGF expression has been reported to be regulated by Wnt signaling (33). However, the present results indicate that activation of either PGE_2 or Wnt signaling alone does not induce VEGF expression in the stomach *in vivo* as well as in the fibroblasts *in vitro*. Importantly, simultaneous stimulation by PGE_2 and Wnt1 also failed to induce VEGF expression in fibroblast cultures. Accordingly, it is possible that promotion of angiogenesis in *Gan* mouse gastric tumors is not simply caused by activation of the PGE_2 and Wnt pathways. Previously, we have shown that simultaneous activation of the PGE_2 and Wnt pathways is responsible for development of gastric adenocarcinoma (16). Therefore, it is possible that tumor cells transformed by PGE_2 and Wnt pathways secondarily express responsible factors other than PGE_2 or Wnt ligands, which activate stromal fibroblasts and bone marrow-derived cells to convert to myofibroblasts and stimulate the expression of angiogenic factors. TNF-α has been reported to induce angiogenesis, and this induction is dependent on IL-8 and basic fibroblast growth factor signaling (34). Moreover, an increased PGE_2 level in the *K19-C2mE* mouse stomach induces inflammatory responses that lead to induction of TNF-α (35). However, the present results suggest that other tumor cell-derived factors than inflammatory cytokines are responsible for the induction of VEGFA in stromal fibroblasts.

It has been shown that CAFs extracted from human breast cancer tissues promote the angiogenesis and growth of cancer cells more significantly than normal mammary fibroblasts (11). Moreover, the α-SMA positive index of CAFs is constitutively higher in culture than that of the counterpart normal fibroblasts, suggesting that CAFs are irreversibly activated by the tumor environment. In this study, a substantial number of α-SMA and tenascin-c positive myofibroblasts were observed in the gastric tumor stroma. However, the α-SMA index of cultured gastric tumor fibroblasts

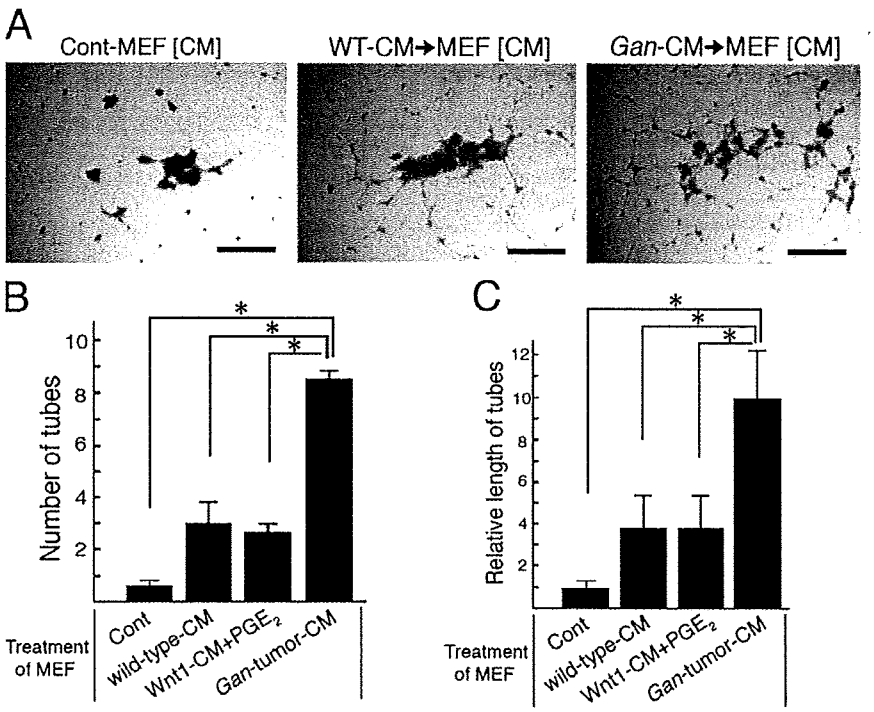

FIGURE 6. **HUVEC tube formation assay.** *A*, representative photographs of HUVEC culture in Matrigel under a dissection microscope (18 h). HUVECs were treated with the secondary CM of MEFs that were stimulated with the primary CM of wild-type epithelial cells (*center*) or *Gan* tumor epithelial cells (*right*). CM of unstimulated MEFs was used as a control (*left*). *Bars* indicate 0.5 mm. *B* and *C*, number of HUVEC tubes and their relative lengths are shown, respectively (mean ± S.D.). *Wnt1-CM+PGE₂* indicates CM of MEFs treated with the primary CM of *K19-Wnt1* epithelial cells and PGE_2 at 1 μM. *, $p < 0.05$.

was at the same level as that from the normal stomach, suggesting that activation of *Gan* mouse tumor fibroblasts is reversible. It is therefore possible that long term interaction between fibroblasts and tumor cells as in human malignancies is required for irreversible education of CAFs.

Interestingly, the responsiveness to conditioned medium of gastric tumor cells is higher in the tumor-derived gastric fibroblasts in comparison with that in the normal stomach fibroblasts (Fig. 4*D* and supplemental Fig. 2*C*). These results suggest that gastric tumor fibroblasts have characteristics that are distinct from normal gastric fibroblasts, even though they are not irreversibly activated. It has been shown that bone-marrow derived cells contribute to myofibroblasts (30, 36) and that inflammatory responses enhance this contribution in tumor stroma (31). Moreover, it has been established that chronic gastritis caused by *Helicobacter pylori* infection is closely associated with gastric cancer development (37), and that the COX-2 pathway is induced in most cases of gastric cancer (17). The present study using *K19-C2mE* mice demonstrated that a subset of gastric myofibroblasts originated from bone marrow cells. Accordingly, it is conceivable that chronic gastritis caused by *H. pylori* infection and subsequent COX-2/PGE_2 induction are involved in the contribution of bone marrow cells to myofibroblasts, which may contributes to distinct characteristics of tumor fibroblasts.

The specific molecules secreted by tumor cells that activate gastric fibroblasts to induce angiogenesis remain to be identified. However, the present results suggest that tumor fibroblasts require stimulation by tumor cells to express angiogenic factors, including VEGFA. Therefore, the suppression of fibroblast activation by the inhibition of tumor cell-derived factors might thus be an effective strategy for the chemoprevention of gastric cancer in combination with the eradication of *H. pylori*. Accordingly, an analysis of gene expression profiles using *Gan* mouse tumors is thus considered to provide important evidence to make it possible to determine the responsible factors.

Acknowledgment—We thank Manami Watanabe for valuable technical assistance.

REFERENCES

1. Tlsty, T. D., and Coussens, L. M. (2006) *Annu. Rev. Pathol.* **1,** 119–150
2. Barcellos-Hoff, M. H., and Ravani, S. A. (2000) *Cancer Res.* **60,** 1254–1260
3. Elenbaas, B., Spirio, L., Koerner, F., Fleming, M. D., Zimonjic, D. B., Donaher, J. L., Popescu, N. C., Hahn, W. C., and Weinberg, R. A. (2001) *Genes Dev.* **15,** 50–65
4. Bhowmick, N. A., Chytil, A., Plieth, D., Gorska, A. E., Dumont, N., Shappell, S., Washington, M. K., Neilson, E. G., and Moses, H. L. (2004) *Science* **303,** 848–851
5. Olumi, A. F., Grossfeld, G. D., Hayward, S. W., Carroll, P. R., Tlsty, T. D., and Cunha, G. R. (1999) *Cancer Res.* **59,** 5002–5011
6. Allinen, M., Beroukhim, R., Cai, L., Brennan, C., Lahti-Domenici, J., Huang, H., Porter, D., Hu, M., Chin, L., Richardson, A., Schnitt, S., Sellers, W. R., and Polyak, K. (2004) *Cancer Cell* **6,** 17–32
7. Sappino, A. P., Skalli, O., Jackson, B., Shurch, W., and Gabbiani, G. (1988) *Int. J. Cancer* **41,** 707–712
8. Adegboyega, P. A., Mifflin, R. C., DiMari, J. F., Saada, J. I., and Powell, D. W. (2002) *Arch. Pathol. Lab. Med.* **126,** 829–836
9. Nakayama, H., Enzan, H., Miyazaki, E., and Toi, M. (2002) *J. Clin. Pathol.* **55,** 741–744
10. Hanahan, D., and Weinberg, R. A. (2000) *Cell* **100,** 57–70
11. Orimo, A., Gupta, P. B., Sgroi, D. C., Arenzana-Seisdedos, F., Delaunay, T., Naeem, R., Carey, V. J., Richardson, A. L., and Weinberg, R. A. (2005) *Cell* **121,** 335–348
12. Shao, J., Sheng, G. G., Mifflin, R. C., Powell, D. W., and Sheng, H. (2006) *Cancer Res.* **66,** 846–855
13. Sonoshita, M., Takaku, K., Sasaki, N., Sugimoto, Y., Ushikubi, F., Narumiya, S., Oshima, M., and Taketo, M. M. (2001) *Nat. Med.* **7,** 1048–1051
14. Seno, H., Oshima, M., Ishikawa, T., Oshima, H., Takaku, K., Chiba, T., Narumiya, S., and Taketo, M. M. (2002) *Cancer Res.* **62,** 506–511
15. Ronnov-Jessen, L., Petersen, O. W., Koteliansky, V. E., and Bissell, M. J. (1995) *J. Clin. Investig.* **95,** 859–873
16. Oshima, H., Matsunaga, A., Fujimura, T., Tsukamoto, T., Taketo, M. M., and Oshima, M. (2006) *Gastroenterology* **131,** 1086–1095
17. Saukkonen, K., Rintahaka, J., Sivula, A., Buskens, C. J., van Rees, B. P., Rio, M. C., Haglund, C., van Lanschot, J. J., Offerhaus, G. J., and Ristimaki, A. (2003) *APMIS* **111,** 915–925
18. Murakami, M., Naraba, H., Tanioka, T., Semmyo, N., Nakatani, Y., Kojima, F., Ikeda, T., Fueki, M., Ueno, A., Oh-ishi, S., and Kudo, I. (2000) *J. Biol. Chem.* **275,** 32783–32792
19. van Rees, B. P., Sivula, A., Thoren, S., Yokozaki, H., Jakobsson, P. J., Offerhaus, G. J., and Ristimake, A. (2003) *Int. J. Cancer* **107,** 551–556
20. Taketo, M. M. (2006) *Oncogene* **25,** 7522–7530
21. Clements, W. M., Wang, J., Sarnaik, A., Kim, O. J., MacDonald, J., Fenoglio-Preiser, C., Groden, J., and Lowy, A. M. (2002) *Cancer Res.* **62,** 3503–3506
22. Tsujii, M., Kawano, S., Tsuji, S., Sawaoka, H., Hori, M., and DuBois, R. N. (1998) *Cell* **93,** 705–716
23. Oshima, H., Oshima, M., Inaba, K., and Taketo, M. M. (2004) *EMBO J.* **23,** 1669–1678
24. Okabe, M., Ikawa, M., Kominami, K., Nakanishi, T., and Nishimune, Y. (1997) *FEBS Lett.* **407,** 313–319
25. Oshima, M., Dinchuk, J. E., Kargman, S. L., Oshima, H., Hancock, B., Kwong, E., Trzaskos, J. M., Evans, J. F., and Taketo, M. M. (1996). *Cell* **87,** 803–809
26. Su, J. L., Shih, J. Y., Yen, M. L., Jeng, Y. M., Chang, C. C., Hsieh, C. Y., Wei, L. H., Yang, P. C., and Kuo, M. L. (2004) *Cancer Res.* **64,** 554–564
27. Matsumoto, K., and Nakamura, T. (2005) *Biochem. Biophys. Res. Commun.* **333,** 316–327
28. Sato, T. N., Tozawa, Y., Deutsch, U., Wolburg-Buchholz, K., Fujiwara, Y., Gendron-Maguire, M., Gridley, T., Wolburg, H., Risau, W., and Qin, Y. (1995) *Nature* **376,** 70–74
29. Burger, J. A., and Kipps, T. J. (2006) *Blood* **107,** 1761–1767
30. Serini, G., and Gabbiani, G. (1999) *Exp. Cell Res.* **250,** 273–283
31. Direkze, N. C., Hodivala-Dilke, K., Jeffery, R., Hunt, T., Poulsom, R., Oukrif, D., Alison, M. R., and Wright, N. A. (2004) *Cancer Res.* **64,** 8492–8495
32. Brittan, M., Chance, V., Elia, G., Poulsom, R., Alison, M. R., MacDonald, T. T., and Wright, N. A. (2005) *Gastroenterology* **128,** 1984–1995
33. Zhang, X., Gaspard, J. P., and Chung, D. C. (2001) *Cancer Res.* **61,** 6050–6054
34. Yoshida, S., Ono, M., Shono, T., Izumi, H., Ishibashi, T., Suzuki, H., and Kuwano, M. (1997) *Mol. Cell. Biol.* **17,** 4015–4023
35. Oshima, M., Oshima, H., Matsunaga, A., and Taketo, M. M. (2005) *Cancer Res.* **65,** 9147–9151
36. Ishii, G., Sangai, T., Oda, T., Aoyahi, Y., Hasebe, T., Kanomata, N., Endoh, Y., Okumura, C., Okuhara, Y., Magae, J., Emura, M., Ochiya, T., and Ochiai, A. (2003) *Biochem. Biophys. Res. Commun.* **309,** 232–240
37. Roder, D. M. (2002) *Gastric Cancer* **1,** Suppl. 5, 5–11

 Related Commentary, page 464

Blocking TNF-α in mice reduces colorectal carcinogenesis associated with chronic colitis

Boryana K. Popivanova,[1] Kazuya Kitamura,[2] Yu Wu,[1] Toshikazu Kondo,[3] Takashi Kagaya,[2] Shiuchi Kaneko,[2] Masanobu Oshima,[4] Chifumi Fujii,[1] and Naofumi Mukaida[1]

[1]Division of Molecular Bioregulation, Cancer Research Institute, and [2]Department of Disease Control and Homeostasis, Graduate School of Medical Science, Kanazawa University, Kanazawa, Japan. [3]Department of Legal Medicine, Wakayama Medical University, Wakayama, Japan. [4]Division of Genetics, Cancer Research Institute, Kanazawa University, Kanazawa, Japan.

The inflammatory bowel disease ulcerative colitis (UC) frequently progresses to colon cancer. To understand the mechanisms by which UC patients develop colon carcinomas, we used a mouse model of the disease whereby administration of azoxymethane (AOM) followed by repeated dextran sulfate sodium (DSS) ingestion causes severe colonic inflammation and the subsequent development of multiple tumors. We found that treating WT mice with AOM and DSS increased TNF-α expression and the number of infiltrating leukocytes expressing its major receptor, p55 (TNF-Rp55), in the lamina propria and submucosal regions of the colon. This was followed by the development of multiple colonic tumors. Mice lacking TNF-Rp55 and treated with AOM and DSS showed reduced mucosal damage, reduced infiltration of macrophages and neutrophils, and attenuated subsequent tumor formation. WT mice transplanted with TNF-Rp55–deficient bone marrow also developed significantly fewer tumors after AOM and DSS treatment than either WT mice or TNF-Rp55–deficient mice transplanted with WT bone marrow. Furthermore, administration of etanercept, a specific antagonist of TNF-α, to WT mice after treatment with AOM and DSS markedly reduced the number and size of tumors and reduced colonic infiltration by neutrophils and macrophages. These observations identify TNF-α as a crucial mediator of the initiation and progression of colitis-associated colon carcinogenesis and suggest that targeting TNF-α may be useful in treating colon cancer in individuals with UC.

Introduction

Ulcerative colitis (UC) is an inflammatory bowel disease characterized by pathological mucosal damage and ulceration, which can involve the rectum and extend proximally (1). The incidence of UC in the United States is about 4–12 per 100,000 and has risen in recent decades. UC typically presents as a relapsing disorder marked by attacks of bloody mucoid diarrhea that sometimes persists for months, only to recur after an asymptomatic interval of months to years (1). UC consistently manifests DNA damage with microsatellite instability in mucosal cells (2). Thus, repetitive relapses and remissions can frequently cause epithelial dysplasia and can eventually progress to invasive cancer (3). Indeed, involvement of the entire colon for longer than 10 years predisposes UC patients to colon cancer, and the risk of cancer is 20- to 30-fold higher in these patients than in a control population (4). Thus, it is desirable to develop measures to prevent cancer development in UC patients based on an understanding of the pathogenesis of colon carcinogenesis in UC at molecular and cellular levels.

Oral administration of dextran sulfate sodium (DSS) solution to rodents is widely employed to recapitulate human UC, because it can cause acute inflammatory reaction and ulceration in the entire colon similar to that observed in UC patients (5). Moreover, repeated oral DSS ingestion alone can cause colon carcinoma in a proportion of mice when the ingestion is of 7 days' duration and is repeated 9 times (6). These observations suggest that the inflammatory response alone can cause colon carcinoma. Azoxymethane (AOM) is also frequently used to induce tumors in the distal colon of rodents by causing O^6-methyl-guanine formation (7). A prior administration of AOM can accelerate and increase the incidence of DSS-induced colon carcinogenesis, as evidenced by the very high incidence of colon cancer (nearly 100%) after 3 subsequent rounds of DSS ingestion (8). Inactivation of the IκB/NF-κB pathway has been associated with reducing colon carcinogenesis induced by the combined treatment of AOM and DSS (9). This observation may mirror the enhanced NF-κB activation seen in human colon adenoma and cancer tissues (10, 11). This suggests that induction of NF-κB by inflammatory stimuli may participate in colon carcinogenesis. However, it still remains to be determined, which molecule(s), if any, aberrantly enhances NF-κB activation during the course of colon carcinogenesis.

NF-κB activation is required for the expression of many proinflammatory molecules including cytokines and adhesion molecules (12). Among these cytokines, TNF-α can further augment NF-κB activation in various cell types after binding to either TNF receptor p55 (TNF-Rp55) or TNF-Rp75 (13). Since TNF-Rp55 is widely expressed on almost all cell types except erythrocytes (14), TNF-Rp55 deficiency has profound effects on endotoxin shock (15) and the skin wound healing process (16). TNF-α was originally identified as a mediator responsible for endotoxin-induced tumor necrosis (17) and was utilized for the treatment of patients with advanced localized solid tumors (18). On the contrary, we observed that liver and lung metastasis were depressed in TNF-Rp55–deficient (TNF-Rp55$^{-/-}$) mice (19, 20), suggesting a crucial contribution of the TNF-α/TNF-Rp55 axis to the development of metastasis. Moreover, TNF-α–deficient mice developed fewer

Nonstandard abbreviations used: AOM, azoxymethane; DSS, dextran sulfate sodium; GSK, glycogen synthase kinase; IKKβ, IκB kinase β; KC, keratinocyte chemoattractant; MCP-1, monocyte chemoattractant protein-1; TNF-Rp55, TNF receptor p55; UC, ulcerative colitis.

Conflict of interest: The authors have declared that no conflict of interest exists.

Citation for this article: *J. Clin. Invest.* 118:560–570 (2008). doi:10.1172/JCI32453.

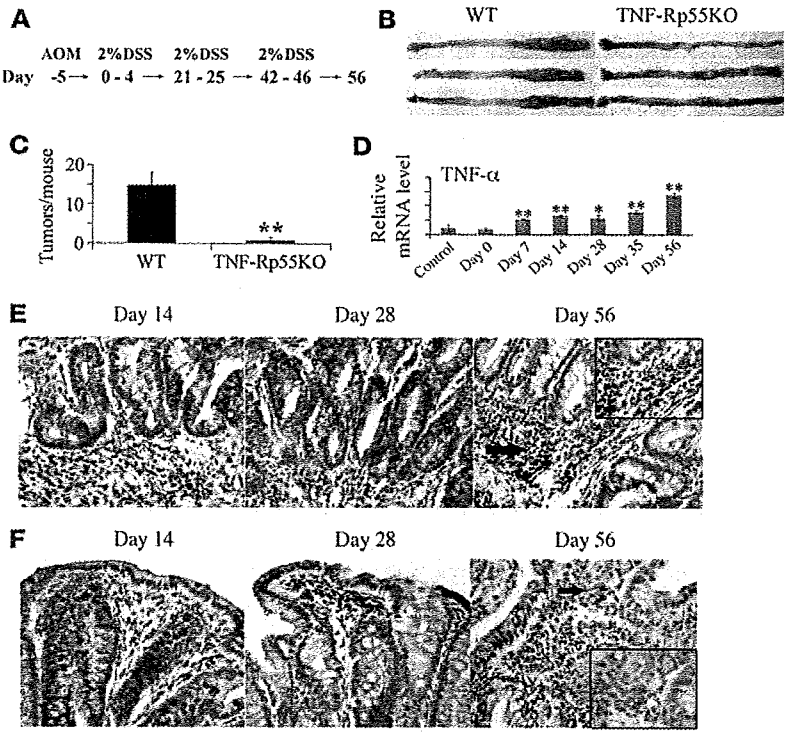

Figure 1
Tumor formation in WT and TNF-Rp55$^{-/-}$ (TNF-Rp55KO) mice after AOM and DSS treatment. (**A**) Schematic overview of this colon carcinogenesis model. (**B**) Macroscopical changes in colon. Colons were removed at day 56 from treated WT and TNF-Rp55$^{-/-}$ mice, and representative results from 10 independent animals are shown here. (**C**) The numbers of tumors. Colons were removed at day 56 to determine the numbers of macroscopic tumors. Each value represents the mean ± SD (n = 10 animals). $^{**}P < 0.01$ versus WT. (**D**). *TNF-α* gene expression in the colons of WT mice. The levels of *TNF-α* mRNA were quantified by quantitative RT-PCR as described in Methods, and normalized to the level of *GAPDH* mRNA. $^{*}P < 0.05$, $^{**}P < 0.01$ versus untreated (control) mice. (**E** and **F**) Immunohistochemical detection of TNF-α and TNF-Rp55 in colons. Colons were obtained from WT mice at the indicated time intervals; insets are higher magnification of the positively stained cells as indicated by arrows. Representative results from 6 independent experiments are shown here (original magnification, ×400; ×1,000 [insets]).

tumors than WT mice when exposed to several types of carcinogens (21). Thus, the TNF-α/TNF-Rp55 axis may actually promote carcinogenesis and its progression.

Here we investigated the roles of the TNF-α/TNF-Rp55 axis in colon carcinogenesis induced by the combined treatment with AOM and DSS by utilizing TNF-Rp55$^{-/-}$ mice and a human TNF-specific antagonist, etanercept, which can block mouse TNF-α activities (22). Our experiments revealed that the combined treatment with AOM and DSS induced the intracolonic expression of TNF-α, which in turn regulated the trafficking of inflammatory cells, a major source of COX-2, thereby resulting in the development and progression of colon cancer.

Results

Enhanced TNF expression in the colon during the course of colon carcinogenesis. Consistent with previous reports (8, 9), a single intraperitoneal injection of the carcinogen AOM, followed by 3 rounds of 2% DSS intake induced the development of multiple tumors in the middle to distal colon of WT mice (Figure 1, B and C). The essential involvement of a transcription factor, NF-κB, in this colon carcinogenesis model (9) prompted us to investigate the intracolonic expression of TNF-α and its receptor because TNF-α is a potent activator of NF-κB (13, 14). TNF-α mRNA was faintly expressed in untreated WT mice, and AOM treatment alone did not enhance *TNF-α* mRNA expression, but subsequent DSS intake augmented *TNF-α* mRNA expression (Figure 1D). We also detected TNF-α protein expression by immunohistochemical analysis mainly in mononuclear cells present in lamina propria and submucosal regions (Figure 1E). Similarly, immunoreactive TNF-α protein was detected in the colons of patients with active UC and advanced colorectal cancer, but not in normal mucosa (Supplemental Figure 1; supplemental material available online with this article; doi:10.1172/JCI32453DS1). Immunohistochemical analysis detected the major receptor for TNF-α, TNF-Rp55, predominantly in leukocytes infiltrating the lamina propria and submucosal regions of the colon during the course of this colon carcinogenesis model (Figure 1F).

Reduced tumor incidence in TNF-Rp55$^{-/-}$ mice. In order to clarify the role of TNF-Rp55 in this colon carcinogenesis model, we treated both WT and TNF-Rp55$^{-/-}$ mice with AOM and DSS in the same manner. During the course of AOM and DSS treatment, WT mice exhibited profound body weight loss and bloody diarrhea, whereas TNF-Rp55$^{-/-}$ mice had less body weight loss and did not have bloody diarrhea (data not shown). There were no apparent differences in macroscopical and microscopical appearance of the colon of untreated WT and TNF-Rp55$^{-/-}$ mice (Figure 2A). In treated WT mice, edema and hyperemia of the middle to distal colon became evident after day 7, and multiple tumors developed in the same region after day 28, whereas these morphological changes were rare in AOM and DSS–treated TNF-Rp55$^{-/-}$ mice (data not shown). Histological analysis consistently demonstrated massive infiltration of leukocytes into the mucosa and edema of the submucosa, with loss of entire crypts and surface epithelium by day 7, particularly in the middle to distal colon of WT mice (Figure 2A). At day 14, mucosal inflammatory cell infiltration persisted and was accompanied by dysplastic glands with hyperchromatic nuclei, decreased mucin production, and dystrophic goblet cells. By days 28 to 35, macroscopically visible adenocarcinomatous lesions developed, and their size and numbers increased progressively thereafter. Moreover, β-catenin accumulated in the nuclei of the tumor cells after day 28 (Figure 2B). On the contrary, TNF-Rp55$^{-/-}$ mice displayed much milder inflammation of the colon during the course of DSS intake and developed fewer adenocarcinomatous lesions and less nuclear β-catenin accumulation (Figure 1C and Figure 2,

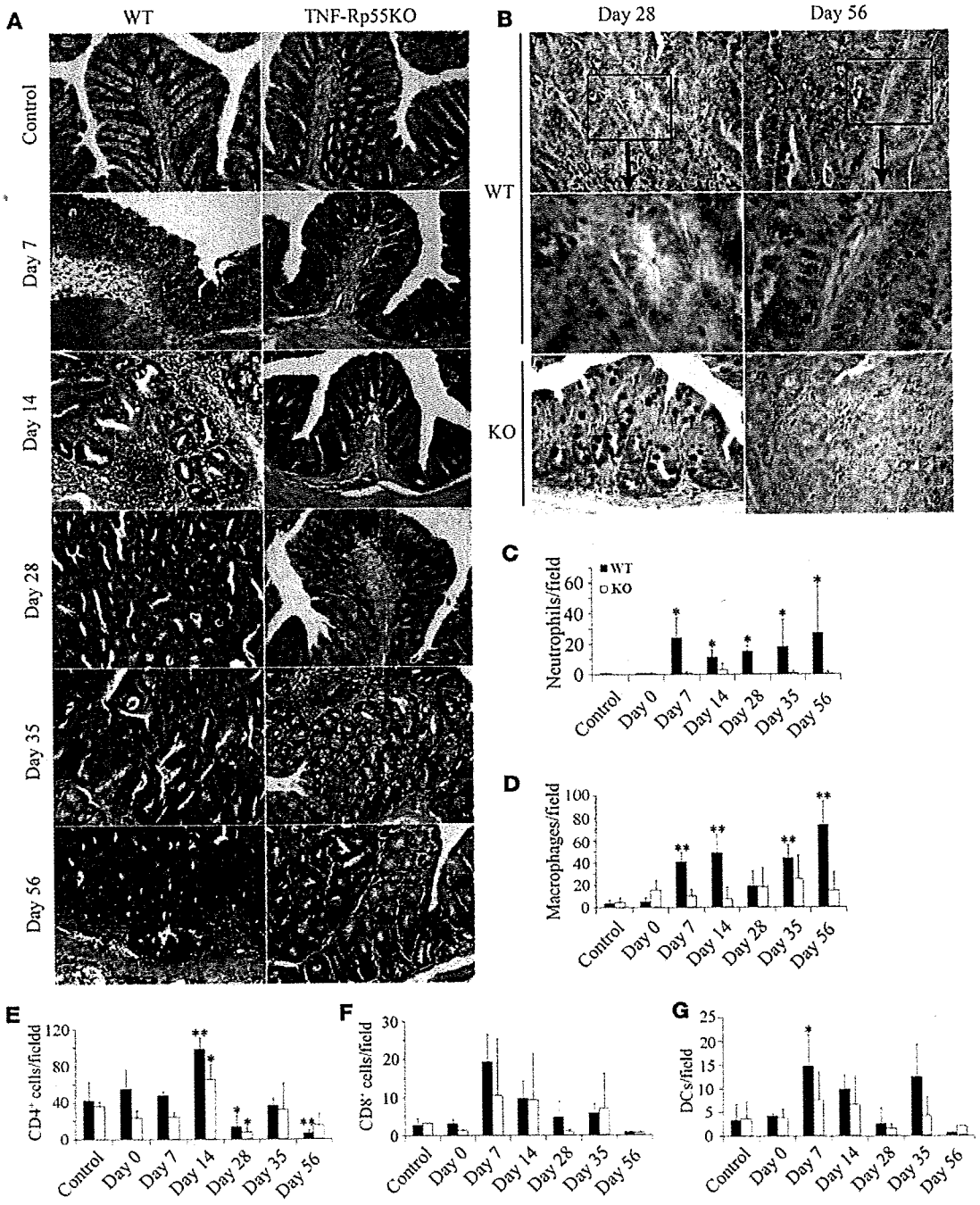

Figure 2

Microscopical analysis of colon tissues. (**A**) Colons were removed at the indicated time intervals, fixed, and stained with hematoxylin and eosin. Representative results from 5 mice are shown here. Original magnification, ×200. (**B**) Immunohistochemical staining for β-catenin. Colons were removed at the indicated time intervals from WT and TNF-Rp55$^{-/-}$ (TNF-Rp55KO) mice and immunostained with anti–β-catenin antibody as described in Methods. Boxed areas in the left panels are shown at higher magnification in the middle panels. Representative results from 3 independent animals are shown here. Original magnification, ×400 (top and bottom rows), ×1,000 (middle row). (**C–G**) The numbers of myeloperoxidase- (**C**), F4/80- (**D**), CD4- (**E**), CD8- (**F**), and DEC205-positive cells (**G**) were counted as described in Methods and are shown here. All values represent the mean ± SD (n = 10 animals). $^{*}P < 0.05$, $^{**}P < 0.01$ versus untreated (control) WT mice.

A and B). Moreover, the numbers of apoptotic cells were transiently increased at day 7 in WT but not TNF-Rp55$^{-/-}$ mice, as revealed by TUNEL assay (Supplemental Figure 2). However, the incidence of apoptotic cells detected in TNF-Rp55$^{-/-}$ mice was similar in level to those in WT mice except on day 7 (Supplemental Figure 2). These observations suggest a crucial role in this model for TNF-Rp55–mediated signals in the development of chronic inflammation and colon carcinoma but not in the apoptotic reactions.

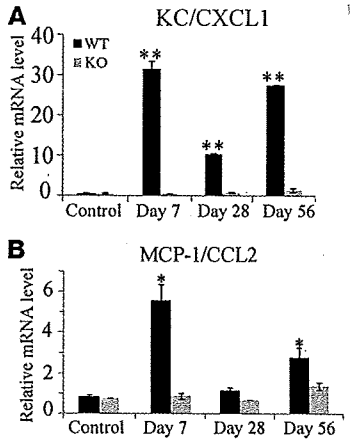

Figure 3
Chemokine gene expression in the colons. Quantitative RT-PCR was performed on total RNAs extracted from the colons at the indicated time intervals as described in Methods. The levels of KC/CXCL1 (**A**) and MCP-1/CCL2 (**B**) mRNA were normalized to GAPDH mRNA levels. Representative results from 5 independent experiments are shown in here. $^{*}P < 0.05$, $^{**}P < 0.01$ versus untreated (control) mice.

Inflammatory cell infiltration. We next proceeded to identify the types of cells that were decreased in the absence of TNF-Rp55 by immunohistochemical analysis. In treated WT mice, neutrophils and macrophages infiltrated into lamina propria and submucosa after day 7 and persisted until day 56 (Supplemental Figure 3). In addition, after day 7 aggregates of CD4-positive lymphocytes and DEC205-positive dendritic cells infiltrated into the lamina propria and submucosa (Supplemental Figure 3). In AOM and DSS-treated TNF-Rp55$^{-/-}$ mice, infiltration by both neutrophils and macrophages was markedly decreased, whereas lymphocyte and dendritic cell infiltration was minimally affected (Figure 2, C–G). TNF-α can augment the expression of the chemokines keratinocyte chemoattractant/CXCL1 (KC/CXCL1) and monocyte chemoattractant protein-1/CCL2 (MCP-1/CCL2), which are chemotactic for neutrophils and macrophages, respectively (23, 24). Indeed, after day 7, gene expression of both chemokines was enhanced in WT mice, but their expression was consistently depressed in TNF-Rp55$^{-/-}$ mice (Figure 3). These observations suggest that TNF-Rp55–mediated signals were responsible for the trafficking of neutrophils and macrophages, at least in part by enhancing the expression of chemokines. Moreover, it is plausible that bone marrow–derived cells, neutrophils and macrophages, can be crucially involved in this colon carcinogenesis model. In order to address the contribution of bone marrow–derived cells, we treated various bone marrow chimeric mice with the same combination of AOM and DSS. TNF-Rp55$^{-/-}$ mice transplanted with WT-derived bone marrow cells developed tumors at a similar level as WT mice transplanted with WT-derived bone marrow cells, but at a higher level than either WT or TNF-Rp55$^{-/-}$ mice transplanted with TNF-Rp55$^{-/-}$ mouse–derived bone marrow cells (Figure 4). These observations suggest that TNF-Rp55–mediated signals act mainly on bone marrow, but not non–bone marrow–derived cells in this carcinogenesis model.

Reduced COX-2 expression in TNF-Rp55$^{-/-}$ mice. Accumulating evidence indicates the causal involvement of COX-2 in colon carcinogenesis. Hence, we examined *COX-2* mRNA expression by real-time RT-PCR. After day 7, intracolonic COX-2 expression was markedly enhanced in treated WT but not TNF-Rp55$^{-/-}$ mice (Figure 5A). COX-2 protein was detected mainly in infiltrating inflammatory cells (Figure 5B), and the numbers of COX-2–positive cells increased from day 7 to day 56 in WT but not TNF-Rp55$^{-/-}$ mice (Figure 5, B and C). Double-color immunofluorescence analysis detected COX-2 protein in F4/80-positive macrophages and to a lesser extent in Ly-6G–positive neutrophils (Figure 5D). These observations suggest that in the absence of TNF-Rp55 the infiltration of macrophages and neutrophils, which are a major source of COX-2, was reduced, leading to decreased COX-2 expression.

Effect of TNF-α antagonist, etanercept, on tumor formation in WT mice. Because the human TNF antagonist, etanercept, can inhibit the biological activity of murine TNF (22), we explored its effects on tumor progression by administering it to mice from day 56 to day 60, after the AOM and 3 cycles of DSS treatments (Figure 6A). Compared with the vehicle-treated group, etanercept treatment reduced the numbers and size of macroscopical tumors remarkably when administered even over this short and delayed time period (Figure 6, B–D). Concomitantly, etanercept treatment reduced intracolonic infiltration by inflammatory cells, particularly neutrophils and macrophages (Figure 6, E and F, and Supplemental Figure 4),

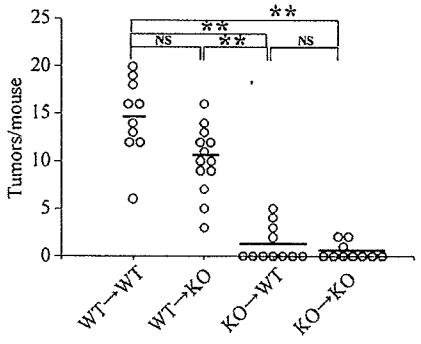

Figure 4
Colon tumor formation in bone marrow chimeric mice. Bone marrow chimeric mice were generated and subjected to AOM+DSS treatment as described in Methods. Colons were removed at day 56, and the tumor numbers were determined macroscopically. The bars represent the median of each group; each symbol represents the tumor numbers of each animal. $^{**}P < 0.01$.

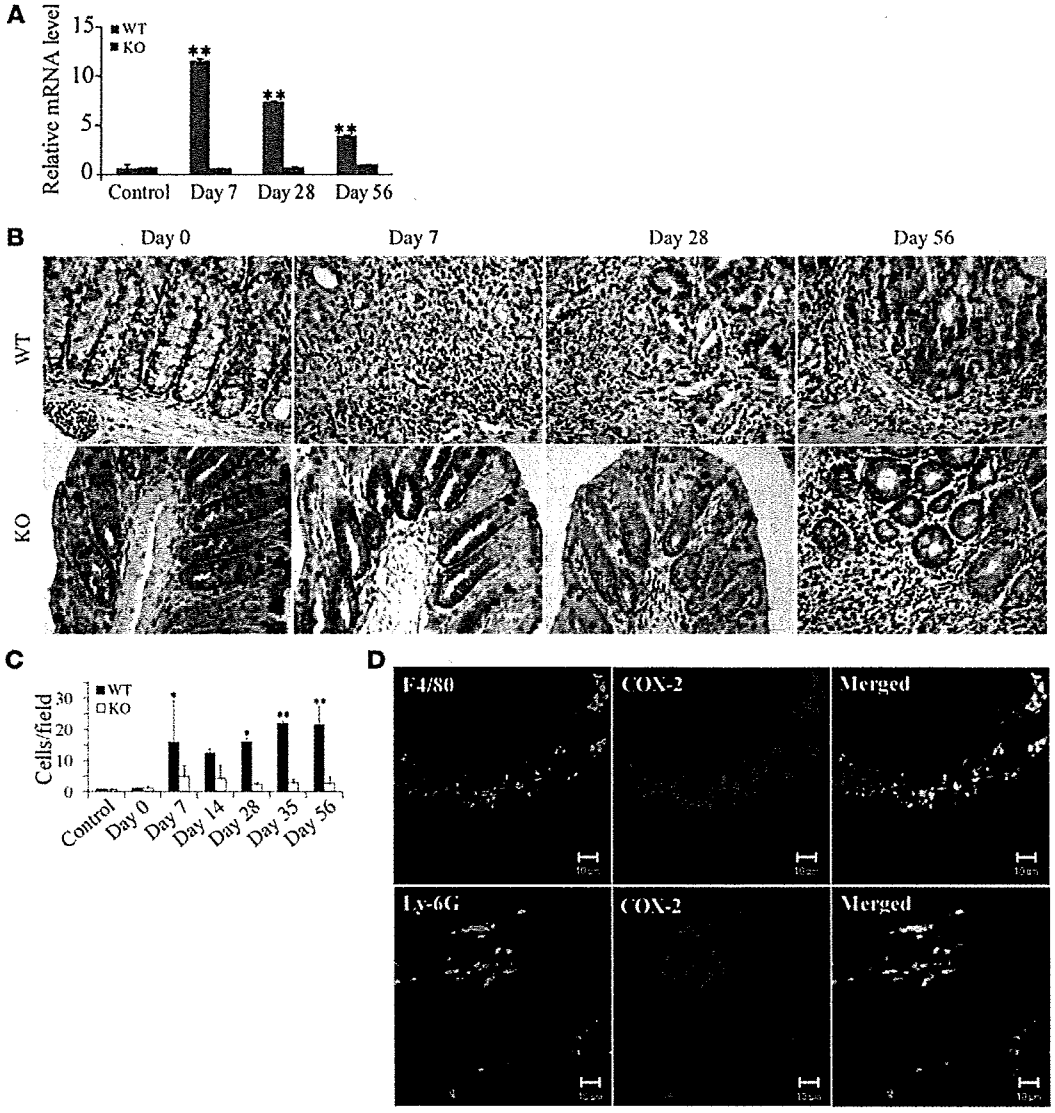

Figure 5

COX-2 expression in the colons. (**A**) Quantitative RT-PCR was performed on total RNAs extracted from the colons at the indicated time intervals as described in Methods. The levels of COX-2 mRNA were normalized to the levels of GAPDH mRNA. $^{**}P < 0.01$ versus untreated (control) mice. (**B–D**) Immunohistochemical and immunofluorescence detection of COX-2–expressing cells. Colons were obtained from WT mice at the indicated time intervals and processed for immunohistochemical analysis using anti–COX-2 antibodies, and representative results from 5 independent animals are shown in **B**. The numbers of COX-2–expressing cells were determined as described in Methods and are shown in **C** and expressed as mean ± SD. $^{*}P < 0.05$, $^{**}P < 0.01$ versus untreated. Double-color immunofluorescence analysis was performed with the combination of anti–COX-2 and anti–F4/80 (**D**, top row) or that of anti–COX-2 and anti-Ly6G antibodies (**D**, bottom row). Representative results from 5 independent experiments are shown here. Original magnification, ×400 (**B**); ×800 (**D**). Scale bars, 10 μm.

together with a decrease in mRNA levels of the neutrophil-tropic chemokine, KC/CXCL1, and the macrophage-tropic chemokine, MCP-1/CCL2 (Figure 6, G and H). Furthermore, etanercept reduced *COX-2* mRNA expression (Figure 7A) and the numbers of COX-2 expressing cells (Figure 7, B and C). Because COX-2–derived PGE_2 is an important stimulant of tumor angiogenesis (25), we next examined the effect of etanercept on the intratumoral vascular density by immunostaining with anti-CD31 antibody. At 56 and 67 days after the initiation of DSS intake, WT mice exhibited a marked increase in vascular densities, and this increment was markedly depressed by etanercept (Figure 7, D and E).

PGE_2 has also been reported to have direct effects on the β-catenin axis (26). This prompted us to evaluate the state of β-catenin in the tumors of mice treated with etanercept. Indeed, etanercept also decreased the nuclear accumulation of β-catenin at the tumor sites (Figure 8, A and B). The amounts of unphosphorylated (active) β-catenin protein were increased in WT mice at days 56 and 67, and etanercept markedly reduced this increase (Figure 8C). Moreover, etanercept markedly decreased the numbers of cytokeratin 20–positive cells (Figure 8, A and D), which represent colon adenocarcinoma cells (27). Takahashi and colleagues observed that in these AOM-induced tumors, the β-*catenin*

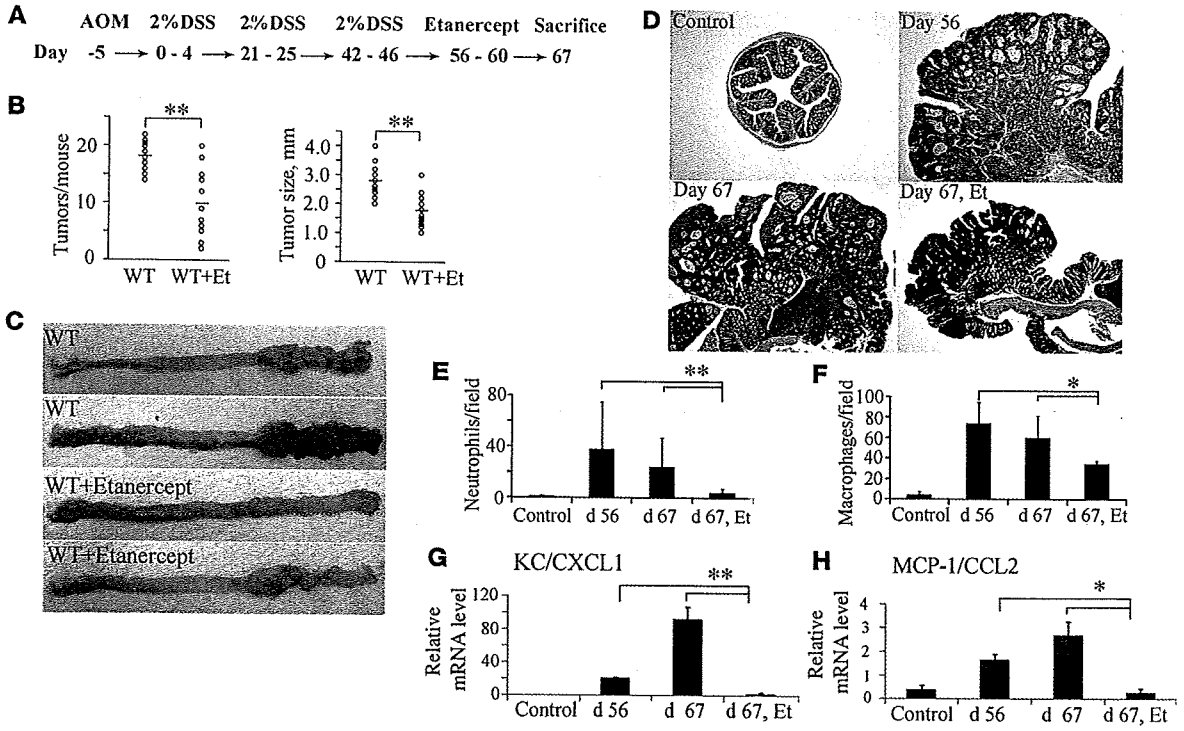

Figure 6

The effects of a TNF antagonist, etanercept, on colon carcinogenesis. (**A**) Schematic overview of etanercept administration. Colons were removed at day 67 after the mice were administered etanercept (Et) or a vehicle control between days 56 and 60. (**B**) The tumor sizes and numbers were determined macroscopically. The bars represent the median of each group. Each symbol represents the tumor numbers of each animal or the average size of the tumors of each animal. (**C**) Macroscopic evaluation of the tumors. Colons were removed on day 67 from WT mice, treated with etanercept or with vehicle. Representative results from 10 independent animals are shown here. Original magnification, ×6. (**D**) Colons were processed for hematoxylin and eosin staining and representative results from 5 independent animals are shown here. Original magnification, ×40. (**E** and **F**) Myeloperoxidase- (**E**) and F4/80-positive cells (**F**) were enumerated as described in Methods. All values represent the mean ± SD (n = 10 animals). $^*P < 0.05$, $^{**}P < 0.01$ versus etanercept-untreated WT mice. (**G** and **H**) Quantitative RT-PCR analysis for KC/CXCL1 (**G**) and MCP-1/CCL2 (**H**) was performed on total RNAs extracted from the colons at the indicated time intervals as described in Methods. KC/CXCL1 and MCP-1/CCL2 mRNA levels were normalized to the levels of GAPDH mRNA. $^*P < 0.05$, $^{**}P < 0.01$ versus etanercept untreated WT mice.

gene, particularly at its glycogen synthase kinase-3β (GSK-3β) phosphorylation sites, mutated more frequently than adenomatous polyposis coli (*APC*) gene (28). Hence, we examined the effects of TNF blockade on the mutations of the GSK-3β phosphorylation sites of the β-*catenin* gene, located in its exon 3. Mutations of β-*catenin* gene were detected in all tumors, and etanercept treatment reduced the mutation frequency markedly from 10/10 positive in the untreated group to 3/10 in the etanercept-treated group (Supplemental Table 1). These observations suggest that blocking of TNF signaling can reverse tumorigenesis even when colon carcinoma is already present, probably by reducing the infiltration of inflammatory cells. Such cells are a major source of COX-2, which is presumed to be involved in both tumor neovascularization and β-catenin activation.

Discussion

During relapses acute attacks of UC cause a massive infiltration of neutrophils and mononuclear cells into the lamina propria and ulceration of colon extending into the submucosa. During remissions of active disease, granulation tissues fill the ulcer craters, accompanied by regeneration of the mucosal epithelium (1, 29). Aminosalicylates, corticosteroids, and cyclosporine are all used to induce remissions and prevent relapse of quiescent disease (29). Despite these medical treatments, UC patients frequently experience relapses and sometimes undergo colectomy. Moreover, recurrent relapses can cause dysplasia of regenerated mucosal epithelium and subsequent progression to frank carcinoma (2, 3). Accordingly, new treatments for UC are needed. A recent clinical trial demonstrated that humanized anti–TNF-α antibody was beneficial for the treatment of moderately to severely active UC patients (30). However, the pathogenic role of TNF-α in UC remains unclear and is particularly so in UC-associated colon carcinogenesis. Hence, we examined the process of chronic colitis–induced colon carcinogenesis by using mice deficient in TNF-Rp55, a major receptor for TNF-α as well as a TNF antagonist, and demonstrated the critical role of the TNF signaling pathway in colon carcinogenesis.

Greten and colleagues have revealed the crucial involvement of the IκB kinase β/NF-κB (IKKβ/NF-κB) in colon carcinogenesis induced by combined treatment with AOM and DSS (9). They further demonstrated that depletion of IKKβ in intestinal epithelial cells increased epithelial apoptosis and concomitantly decreased tumor incidence without affecting tumor size and inflammation.

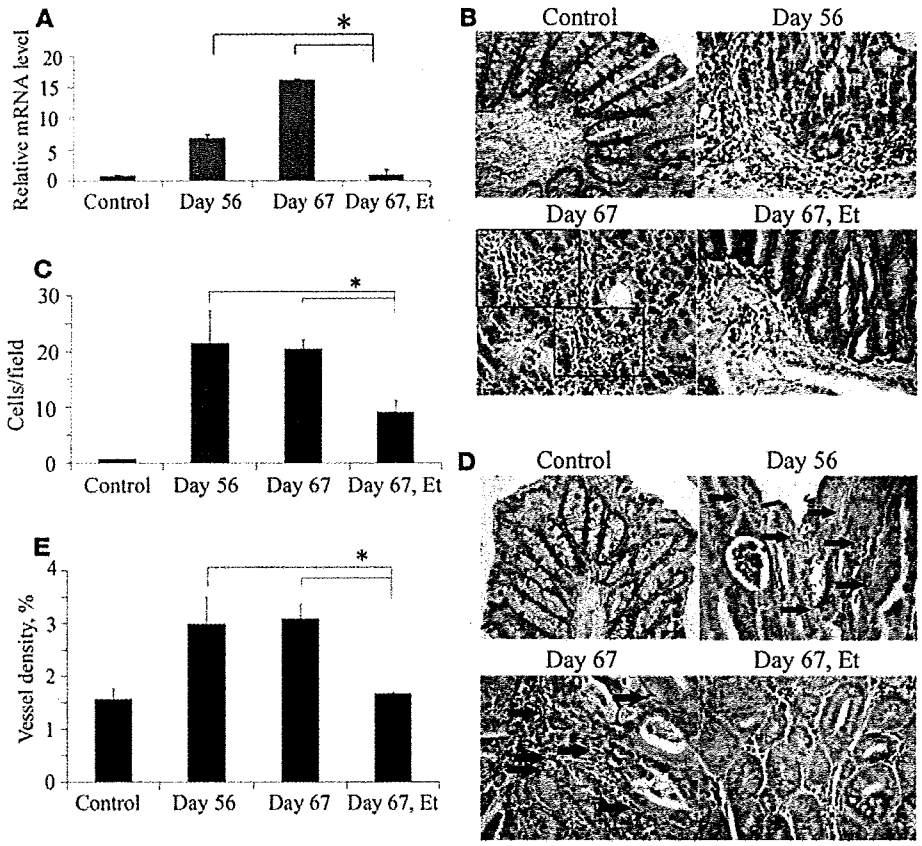

Figure 7

The effect of etanercept on COX-2 expression and angiogenesis. (**A**) Quantitative RT-PCR analysis for COX-2 was performed on total RNAs extracted from the colons at the indicated time intervals as described in Methods. The levels of COX-2 mRNA were normalized to the levels of GAPDH mRNA. *$P < 0.05$ versus untreated (control) mice. (**B** and **C**) Immunohistochemical analysis with anti–COX-2 antibody was performed on colons from WT mice as described in Methods. Boxed area in **B** is shown at higher magnification. Representative results from 5 independent animals are shown in **B** (original magnification, ×400; ×1,000 [insets]). The numbers of COX-2 expressing cells were determined on 5 independent animals as described in Methods. The mean and SD were calculated on all values and are shown in **C**. *$P < 0.05$ versus untreated mice. (**D** and **E**) Colon tissues were immunostained with anti-CD31 antibody as described in Methods. Representative results from 5 independent animals are shown in **D**. Arrows in **D** indicate capillary vessels. Original magnification, ×400. The vascular densities were determined as described in Methods and are shown in **E**. All values represent the mean ± SD. *$P < 0.05$ versus untreated mice.

In contrast, depleting IKKβ in myeloid cells reduced tumor size and inflammation without affecting apoptosis (9). However, in our model, epithelial cell apoptosis was transiently increased at day 7 in WT mice, and this increase was absent in TNF-Rp55$^{-/-}$ mice (Supplemental Figure 2). Moreover, in the absence of TNF-Rp55, colonic inflammation was reduced as was the tumor incidence and size. Furthermore, both TNF-α and TNF-Rp55 were expressed mainly by infiltrating cells but not epithelial cells. Thus, it is plausible to speculate that endogenously produced TNF-α activated NF-κB in inflammatory cells by interacting with TNF-Rp55 in an autocrine/paracrine manner, and caused extensive colonic inflammation, thereby inducing carcinogenesis in this model.

In most cases of colon carcinogenesis, the earliest event is the loss of the *APC* gene, resulting in nuclear β-catenin accumulation (31), as we observed in tumor tissues in this study. Carcinoma progression occurs due to chromosomal instability, which results in a stepwise accumulation of mutations in a number of oncogenes and tumor suppressor genes. TNF-α has been proposed to be a potent mutagen based on its capacity to induce the generation of ROS and subsequent genetic instability in various types of cells (32, 33). This assumption may be further corroborated by the observations that the incidence of chemically induced skin carcinomas was markedly reduced in TNF-α–deficient mice (21) or by the administration of neutralizing antibody to TNF-α (34). Thus, blocking of TNF activities may prevent ROS generation, thereby dampening the initiation of colon carcinogenesis in our model.

The progression to invasive cancer requires the induction of tumor vasculature, termed the angiogenic switch (35). Given the angiogenic activities of TNF-α (36, 37), blocking of TNF signals may prevent the angiogenic switch as evidenced by reduced tumor neovascularization with etanercept administration. Moreover, several lines of evidence implied that infiltrating macrophages and/or neutrophils had a crucial role in the angiogenic switch (38, 39). We observed that macrophages and neutrophils infiltrated into tumor tissues, exhibiting enhanced expression of chemokines active for macrophages and neutrophils, and that blocking of TNF signals reduced macrophage and neutrophil infiltration, together with reduced chemokine gene expression and tumor neovascularization. Furthermore, some of these chemokines can also enhance endothelial cell proliferation (40). Because TNF-α can induce the expression of these chemokines in vitro and in vivo (23, 24), the TNF-α/TNF receptor axis may regulate the angiogenic switch directly or indirectly by inducing the expression of chemokines, which can induce both the proliferation of endothelial cells and the infiltration of inflammatory cells, another rich source of angiogenic factors.

Epidemiological studies demonstrated that nonsteroidal anti-inflammatory drugs (NSAIDs) are effective in reducing the incidence of colon cancer (41, 42). NSAIDs can inhibit the enzymatic activities of both COX-1 and COX-2, but only COX-2 expression was enhanced in colon carcinoma tissues (43). Moreover, *COX-2* gene ablation or the administration of a selective COX-2 inhibitor suppressed the intestinal polyposis observed in *APC*-deficient mice (44). COX-2 converts arachidonic acid to PGH_2, which is

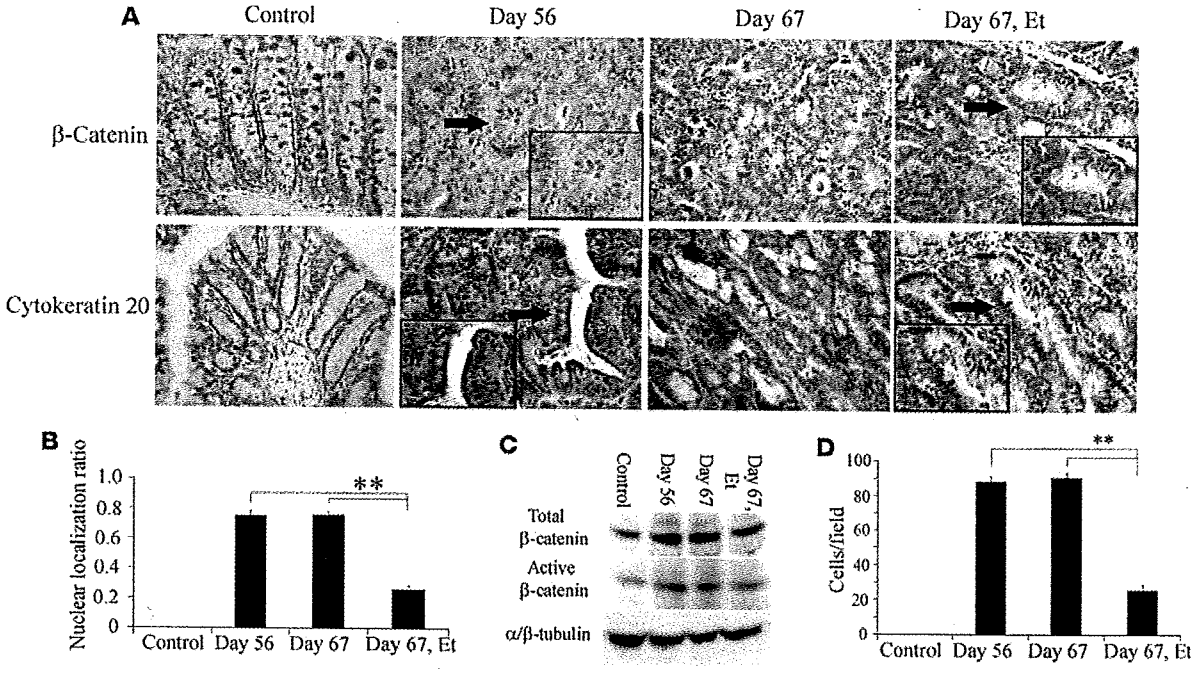

Figure 8

The effect of etanercept on β-catenin nuclear translocation. (**A**) Colons were immunostained with anti–β-catenin (upper panels) or anti–cytokeratin 20 antibody (lower panels) and representative results from 5 independent animals are shown. Insets are higher magnifications of the positively stained cells, indicated by arrows. Original magnification, ×400; ×1,000 (insets). (**B**) The β-catenin nuclear localization ratio was determined as the ratio of the numbers of tumor nuclei with β-catenin localization to the total number of tumor nuclei per field. At least 5 randomly chosen fields at ×400 magnification were examined. All values represent the mean ± SD. $^{**}P < 0.01$ versus etanercept untreated WT mice. (**C**) Immunoblotting analysis with anti–β-catenin antibodies was performed on cell lysates from colon tissues as described in Methods. Representative results from 3 independent experiments are shown here. (**D**) The numbers of cytokeratin 20–positive cells were determined on 5 randomly chosen visual fields at ×400 magnification. All values represent the mean ± SD. $^{**}P < 0.01$ versus etanercept untreated WT mice.

further converted to other PGs including PGE_2 and thromboxanes (25). Several lines of evidence implicate PGE_2 as an essential mediator for angiogenesis in colon carcinogenesis (25, 45–47). In our model, we also observed that COX-2 mRNA expression was enhanced by DSS ingestion and that COX-2 proteins were detected in F4/80-positive macrophages and Ly-6G–positive neutrophils, similar to what has been observed in human and mouse colon cancer tissues (43, 48, 49). Moreover, *TNF-Rp55* gene ablation and TNF antagonist administration reduced both COX-2 expression and tumor angiogenesis. Thus, TNF may also enhance tumor angiogenesis by inducing the infiltration of COX-2–expressing macrophages and neutrophils.

Accumulating evidence suggests that PGE_2 has direct effects in enhancing colonic epithelial cell survival. PGE_2 transactivated nuclear peroxisome proliferator–activated receptor δ through PI3K/Akt signaling, resulting in promoted cell survival and intestinal adenoma formation (50). Moreover, PGE_2 transactivated hepatocyte growth factor (HGF) receptor and induced urokinase-type plasminogen activator receptor mRNA, thereby enhancing colon cancer cell invasive capacity (51). It is of interest that PGE_2-induced HGF receptor transactivation also induced nuclear translocation of β-catenin (51), suggesting a connection between PGE_2 and the Wnt/β-catenin axis. Supporting this notion, upon binding to its specific receptor, EP2, PGE_2 activated the Wnt/β-catenin axis in colon cancer cells through the phosphoinositide 3-kinase/Akt-G protein α_s-axin signaling axis resulting in the promotion of cell growth (26). Moreover, PGE_2 increased the phosphorylation of GSK-3 and induced the accumulation of β-catenin and the expression of its transcription partner, T cell factor–4, thereby inducing the β-catenin/T cell factor-dependent gene transcription in colon cancer cells (52). Thus, COX-2–derived PGE_2 can directly regulate colon carcinogenesis by regulating Wnt signaling pathway, which has a crucial role in colon carcinogenesis. We observed, on the other hand, that etanercept consistently reduced COX-2 expression and the amount of nuclear β-catenin as well as neovascularization, even when it was administered after macroscopic tumor formation. Therefore, TNF blocking may retard the progression of colon carcinomas by reducing COX-2 expression and eventually inhibiting the Wnt signaling pathway.

Our present observations have revealed the crucial involvement of TNF-α in the initiation of chronic inflammation-mediated colon carcinogenesis. Moreover, blocking of TNF-α reversed carcinoma progression, even after colon carcinoma was established. TNF-α blocking agents can have serious adverse effects including the induction of bacterial, tuberculosis, and opportunistic infections, but the incidence is low (30, 53). Thus, drugs targeting TNF-α may be useful for the treatment of cancers, particularly those arising from chronic inflammation.

Methods

Reagents and antibodies. AOM and DSS (MW 36,000–50,000) were purchased from Sigma-Aldrich and MP Biochemicals Inc., respectively. A specific

TNF antagonist, etanercept, was purchased from Wyeth Pharmaceutical Japan. Rat anti-F4/80, rat anti-CD3, and rat anti-DEC205 antibodies were obtained from Serotec. Goat anti-COX-2 antibodies and rabbit anti-myeloperoxidase antibodies were obtained from Santa Cruz Biotechnology and Neomarkers, respectively. Rabbit anti-β-catenin, anti-active β-catenin, and rabbit anti-α/β-tubulin antibodies were from Sigma-Aldrich, Upstate, and Cell Signaling Technology Inc., respectively. Rabbit polyclonal anti-TNF-Rp55, mouse monoclonal anti-human TNF-α, rabbit polyclonal anti-CD31, and mouse monoclonal antibody to cytokeratin 20 were obtained from Abcam. Rabbit polyclonal anti-TNF-α antibody was prepared by immunizing rabbits with a recombinant mouse TNF-α protein (54). ImmunoPure peroxidase-conjugated goat anti-mouse and goat anti-rabbit antibodies were obtained from Pierce Biotechnology Inc. Alexa Fluor 546 donkey anti-goat and Alexa Fluor 488 donkey anti-rat antibodies were obtained from Molecular Probes. Other antibodies were obtained from BD Bioscience – Pharmingen unless otherwise indicated.

Animal experiments. Pathogen-free 8- to 12-week old female WT BALB/c mice and TNF-Rp55$^{-/-}$ mice on a BALB/c genetic background, were housed under specific pathogen-free conditions with free access to food and water during the course of experiments (16, 19, 20). Mice were injected intraperitoneally with 12 mg/kg body weight of AOM dissolved in physiological saline. Five days later, 2% DSS was given in the drinking water over 5 days, followed by 16 days of regular water. This cycle was repeated a total of 3 times (Figure 1A). Body weight was measured every week, and the animals were sacrificed at the indicated time intervals for macroscopical inspection, histological analysis, and total RNA extraction. In some experiments, WT mice were injected with etanercept at a dose of 3 mg/kg body weight every day from day 56 to day 60 (Figure 6A). All animal experiments were approved by the Committee on Animal Experimentation of Kanazawa University and performed in compliance with the university's Guidelines for the Care and Use of Laboratory Animals.

Bone marrow chimeric mice generation. Cell suspensions from male WT or TNF-Rp55$^{-/-}$ bone marrow were prepared from femurs and tibias, filtered, and counted. Female WT or TNF-Rp55$^{-/-}$ mice received a single intravenous injection of 1×10^7 bone marrow cells, after being irradiated with 8.5-Gy followed by 4.25-Gy x-rays (MPR-1520R; Hitachi) 4 hours later. The following groups of chimeric mice were generated: WT to WT, WT to TNF-Rp55$^{-/-}$, TNF-Rp55$^{-/-}$ to WT, and TNF-Rp55$^{-/-}$ to TNF-Rp55$^{-/-}$ mice. Genomic DNA was extracted from blood, and bone marrow chimerism was determined 4 weeks later by PCR for the Y chromosome–linked *Sry* gene (forward, 5′-TGGGACTGGTGACAATTGTC-3′; reverse, 5′-GAGTACAG-GTGTGCAGCTCT-3′).

Histopathological and immunohistochemical analyses of mouse colon tissues. Resected mouse colon tissues were fixed in 10% formalin neutral buffer solution (Wako) for paraffin embedding or were immediately frozen in Tissue-Tek O.C.T. compound (Sakura Fine Technical Co.) and stored at -80°C. Paraffin-embedded sections were cut at 5 μm and stained with hematoxylin and eosin solution. Paraffin-embedded sections were additionally deparaffinized for immunohistochemical detection of cells positively stained for β-catenin, TNF-Rp55, MPO, F4/80, CD3, CD31, or cytokeratin 20. Frozen sections were fixed in 4% paraformaldehyde/PBS for 15 minutes for immunohistochemical detection of cells positively stained for mouse TNF-α, CD4, CD8, or DEC205. Endogenous peroxidase activity was blocked using 3% H_2O_2 for 5 minutes, followed by incubation with Non-Specific Staining Blocking reagent (DakoCytomation) for 10 minutes. The sections were incubated with the optimal dilutions of anti-MPO, anti-F4/80, anti-CD3, anti-CD4, anti-CD8, anti-DEC205, anti-β-catenin, anti-COX-2, anti-CD31, or anti-cytokeratin 20 antibodies overnight at 4°C. MPO-, β-catenin-, TNF-α-, TNF-Rp55-, and anti-CD31-positive cells were detected with HRP-labeled anti-rabbit polymer (EnVision+ System; DakoCytomation), while F4/80- and CD3-positive cells were detected using Catalyzed Signal Amplification (CSA) System (DakoCytomation). Immune complexes were visualized with Peroxidase Substrate DAB kit (Vector Laboratories Inc.). CD4-, CD8-, DEC205-, and COX-2–positive cells were detected by the incubation with anti-rat or anti-goat biotinylated IgG (1:200; DakoCytomation). Detection of cytokeratin 20 was performed with Vector M.O.M. Immunodetection kit (Vector Laboratories Inc.), which was used according to the manufacturer's instructions. The resultant immune complexes were visualized by ABC Elite kit (Vector Laboratories Inc.) and Peroxidase Substrate DAB kit (Vector Laboratories Inc.) according to the manufacturer's instructions. Finally, the slides were counterstained with hematoxylin, dehydrated, and coverslipped. Positive cells were enumerated on 5 randomly chosen visual fields at ×400 magnification. The pixel numbers of CD31-positive areas were measured on 5 randomly chosen visual fields at ×200 magnification with the aid of Adobe Photoshop software. For double-color immunofluorescence analysis, the sections were incubated with the combination of anti-COX-2 and anti-F4/80 or with anti-COX-2 and anti-Ly-6G antibodies at 4°C, overnight. Alexa Fluor 546 donkey anti-goat and Alexa Fluor 488 donkey anti-rat antibodies were used as secondary antibodies. Immunofluorescence was visualized on a Carl Zeiss Laser Scanning Microscope 510.

Immunohistochemical detection of TNF-α in human colon tissues. The tissues were obtained upon biopsy from patients with UC and colorectal cancer with an informed consent and with approval from the Human Subjects Research Ethical Committee of Kanazawa University Hospital. The tissues were fixed and paraffin-embedded and were cut at 5 μm. Paraffin-embedded sections were additionally deparaffinized for immunohistochemical analysis, using the combination of anti-human TNF-α mouse monoclonal antibody and CSA system.

TUNEL assay. Paraffin-embedded sections were stained with In situ Apoptosis Detection Kit (TaKaRa Bio Inc.), according to the manufacturer's instructions, to detect apoptotic cells. TUNEL-positive cells were counted on 5 randomly chosen visual fields at ×400 magnification.

Quantitative RT-PCR. Total RNA was extracted from colon tissues with RNA-Bee (Tel-Test Inc.) and 2.5 μg of RNA was reverse-transcribed using ReverTraAce (Toyobo) and random primers as described previously. Real-time PCR was performed on Applied Biosystems StepOne Real-Time PCR System (Applied Biosystems) using the comparative C_t quantitation method. TaqMan Gene Expression Assays (Applied Biosystems) containing specific primers (accession numbers: TNF-α–Mm00443258_m1, KC/CXCL1–Mm00433859_m1, MCP-1/CCL2–Mm00441242_m1, COX-2–Mm00478374_m1, GAPDH–Mm99999915_g1), TaqMan MGB probe (FAM dye-labeled), and TaqMan Fast Universal PCR Master Mix were used with 10 ng of cDNA to detect and quantify the expression levels of TNF-α, KC/CXCL1, MCP-1/CCL2, and COX-2 in mouse colon tissues. GAPDH was amplified as internal control. C_t values of GAPDH were subtracted from C_t values of the target genes (ΔC_t). ΔC_t values of treated mice were compared with ΔC_t values of untreated animals. Reactions were done at 95°C for 20 seconds followed by 40 cycles of 95°C for 1 second and 60°C for 20 seconds, 60°C, 20 seconds — 40 cycles.

DNA sequencing and mutation analysis of β-catenin gene. After sequential treatment with AOM and DSS, WT mice were injected with either vehicle or etanercept every day from day 56 to day 60 (Figure 6A). Tumors were obtained at day 67 and embedded in paraffin. Genomic DNA was extracted from paraffin-embedded tumor sections by using NucleoSpin Tissue Kit (Macherey-Nagel Inc.) according to the manufacturer's instructions. Exon 3 of the β-catenin gene, containing the consensus sequence for GSK-3β phosphorylation, was amplified by PCR, using specific primers (forward, 5′-GCTGACCTGATGGAGTTGGA-3′, reverse, 5′-GCTACTTGCTCTTGC-GTGAA-3′) and the following thermal cycling parameters: 94°C, 5 min-

utes; followed by 35 cycles at 94°C, 45 seconds, 55°C, 1 minute, and 72°C, 1 minute; followed by 72°C, 5 minutes. PCR products were subcloned into pSTBlue-1 vector (AccepTor vector; Novagen) and sequenced using BigDye Terminator Ver. 3.1 Cycle Sequencing kit (Applied Biosystems) on an ABI PRISM 3100-Avant Genetic Analyzer (Applied Biosystems).

Immunoblotting analysis. Colon tissues were homogenized and sonicated in RIPA lysis buffer (Santa Cruz Biotechnology Inc.), supplemented with protease inhibitors. After centrifugation at 20,000 *g* for 15 minutes, 30 μg of the supernatants were separated on 10% SDS-polyacrylamide gel and transferred onto an Immobilon-P Transfer membrane (Millipore). After being blocked with 5% skim milk, the membrane was incubated with antibodies to total β-catenin (1:1,000) and active β-catenin (1:500). Rabbit anti-α/β-tubulin antibody (1:1,000) was used as an internal control. ImmunoPure peroxidase-conjugated anti-mouse or anti-rabbit IgG were used as secondary antibodies. The blotted membrane was then treated with the Super Signal West Dura Extended Duration Substrate (Pierce Biotechnology Inc.) and signals were detected by LAS-3000 mini CCD camera (Fuji Film).

Statistics. The means ± SD were calculated for all parameters determined. Statistical significance was evaluated using 1-way ANOVA, followed by Fisher's protected least significant difference test. *P* values less than 0.05 were considered statistically significant.

Acknowledgments

We would like to express our gratitude to Joost J. Oppenheim (National Cancer Institute–Frederick) for his critical review and editing of the manuscript.

Received for publication April 20, 2007, and accepted in revised form November 28, 2007.

Address correspondence to: Naofumi Mukaida, Division of Molecular Bioregulation, Cancer Research Institute, Kanazawa University, 13-1 Takara-machi, Kanazawa 920-0934, Japan. Phone: 81-76-265-2767; Fax: 81-76-234-4520; E-mail: naofumim@kenroku.kanazawa-u.ac.jp.

Kazuya Kitamura's present address is: Mucosal Immunology Section, Laboratory of Molecular Immunology, NIAID, NIH, Bethesda, Maryland, USA.

Chifumi Fujii's present address is: Department of Integrative Physiology and Biosystem Control, Graduate School of Medicine, Shinshu University, Matsumoto, Japan.

1. Fiocchi, C. 1998. Inflammatory bowel disease: Etiology and pathogenesis. *Gastroenterology.* **115**:182–205.
2. Risques, R.A., Rabinovitch, P.S., and Brentnall, T.A. 2006. Cancer surveillance in inflammatory bowel disease: new molecular approaches. *Curr. Opin. Gastroenterol.* **22**:382–390.
3. Ullman, T., Croog, V., Harpaz, N., Sachar, D., and Itzkowitz, S. 2003. Progression of flat low-grade dysplasia to advanced neoplasia in patients with ulcerative colitis. *Gastroenterology.* **125**:1311–1319.
4. Dobbins, W.O., 3rd. 1984. Dysplasia and malignancy in inflammatory bowel disease. *Annu. Rev. Med.* **35**:33–48.
5. Okayasu, I., et al. 1990. A novel method in the induction of reliable experimental acute and chronic ulcerative colitis in mice. *Gastroenterology.* **98**:694–702.
6. Okayasu, I., et al. 2002. Dysplasia and carcinoma development in a repeated dextran sulfate sodium-induced colitis model. *J. Gastroenterol. Hepatol.* **17**:1078–1083.
7. Boivin, G.P., et al. 2003. Pathology of mouse models of intestinal cancer: consensus report and recommendations. *Gastroenterology.* **124**:762–777.
8. Okayasu, I., Ohkusa, T., Kajiura, K., Kanno, J., and Sakamoto, S. 1996. Promotion of colorectal neoplasia in experimental murine ulcerative colitis. *Gut.* **39**:87–92.
9. Greten, F.R., et al. 2004. IKKβ links inflammation and tumorigenesis in a mouse model of colitis-associated cancer. *Cell.* **118**:285–296.
10. Lind, D.S., et al. 2001. NF-κB is upregulated in colorectal cancer. *Surgery.* **130**:363–369.
11. Hardwick, J.C., van den Brink, G.R., Offerhaus, G.J., van Deventer, S.J., and Peppelenbosch, M.P. 2001. NF-κB, p38 MAPK and JNK are highly expressed and active in the stroma of human colonic adenomatous polyps. *Oncogene.* **20**:819–827.
12. Li, Q., Withoff, S., and Verma, I.M. 2005. Inflammation-associated cancer: NF-kappaB is the lynchpin. *Trends Immunol.* **26**:318–325.
13. Liu, Z.G. 2005. Molecular mechanism of TNF signaling and beyond. *Cell Res.* **15**:24–27.
14. Tracey, K.J. 1994. Tumor necrosis factor-alpha. In *The cytokine handbook.* 2nd edition. A. Thomson, editor. Academic Press. London, United Kingdom. 289–304.
15. Pfeffer, K., et al. 1993. Mice deficient for the 55 kd tumor necrosis factor receptor are resistant to endotoxic shock, yet succumb to L. monocytogenes infection. *Cell.* **73**:457–467.
16. Mori, R., Kondo, T., Oshima, T., Ishida, Y., and Mukaida, N. 2002. Accelerated wound healing in tumor necrosis factor receptor p55-deficient mice with reduced leukocyte infiltration. *FASEB J.* **16**:963–974.
17. Bazzoni, F., and Beutler, B. 1996. The tumor necrosis factor ligand and receptor families. *N. Engl. J. Med.* **334**:1717–1725.
18. Senzer, N., et al. 2004. TNFerade biologic, an adenovector with a radiation-inducible promoter, carrying the human tumor necrosis factor alpha gene: a phase I study in patients with solid tumors. *J. Clin. Oncol.* **22**:592–601.
19. Kitakata, H., et al. 2002. Essential roles of tumor necrosis factor receptor p55 in liver metastasis of intrasplenic administration of colon 26 cells. *Cancer Res.* **62**:6682–6687.
20. Tomita, Y., et al. 2004. Spontaneous regression of lung metastasis in the absence of tumor necrosis factor receptor p55. *Int. J. Cancer.* **112**:927–933.
21. Moore, R.J., et al. 1999. Mice deficient in tumor necrosis factor-α are resistant to skin carcinogenesis. *Nat. Med.* **5**:828–831.
22. Liu, R., Bal, H.S., Desta, T., Behl, Y., and Graves, D.T. 2006. Tumor necrosis factor-α mediates diabetes-enhanced apoptosis of matrix-producing cells and impairs diabetic healing. *Am. J. Pathol.* **168**:757–764.
23. Shiratori, Y., et al. 1994. Modulation of KC/gro protein (interleukin-8 related protein in rodents) release from hepatocytes by biologically active mediators. *Biochem. Biophys. Res. Commun.* **203**:1398–1403.
24. Marra, F., Valente, A.J., Pinzani, M., and Abboud, H.E. 1993. Cultured human liver fat-storing cells produce monocyte chemotactic protein-1. Regulation by proinflammatory cytokines. *J. Clin. Invest.* **92**:1674–1680.
25. Iniguez, M.A., Rodriguez, A., Volpert, O.V., Fresno, M., and Redondo, J.M. 2003. Cyclooxygenase-2: a therapeutic target in angiogenesis. *Trends Mol. Med.* **9**:73–78.
26. Castellone, M.D., Teramoto, H., Williams, B.O., Druey, K.M., and Gutkind, J.S. 2005. Prostaglandin E_2 promotes colon cancer cell growth through a G_s-axin-β-catenin signalling axis. *Science.* **310**:1504–1510.
27. Berezowski, K., Stastny, J.F., and Kornstein, M.J. 1996. Cytokeratins 7 and 20 and carcinoembryonic antigen in ovarian and colonic carcinoma. *Mod. Pathol.* **9**:426–429.
28. Takahashi, M., and Wakabayashi, K. 2004. Gene mutations and altered gene expression in azoxymethane-induced colon carcinogenesis in rodents. *Cancer Sci.* **95**:475–480.
29. Hanauer, S.B. 2004. Medical therapy for ulcerative colitis 2004. *Gastroenterology.* **126**:1582–1592.
30. Rutgeerts, P., et al. 2005. Infliximab for induction and maintenance therapy for ulcerative colitis. *N. Engl. J. Med.* **353**:2462–2476.
31. Takayama, T., et al. 2001. Analysis of K-ras, APC, and beta-catenin in aberrant crypt foci in sporadic adenoma, cancer, and familial adenomatous polyposis. *Gastroenterology.* **121**:599–611.
32. Babbar, N., and Casero, R.A., Jr. 2006. Tumor necrosis factor-α increases reactive oxygen species by inducing spermidine oxidase in human lung epithelial cells: a potential mechanism for inflammation-induced carcinogenesis. *Cancer Res.* **66**:11125–11130.
33. Yan, B.Y., et al. 2006. Tumor necrosis factor-α is a potent endogenous mutagen that promotes cellular transformation. *Cancer Res.* **66**:11565–11570.
34. Scott, K.A., et al. 2003. An anti-tumor necrosis factor-α antibody inhibits the development of experimental skin tumors. *Mol. Cancer Ther.* **2**:445–451.
35. Bergers, G., and Benjamin, L.E. 2003. Tumorigenesis and the angiogenic switch. *Nat. Rev. Cancer.* **3**:401–410.
36. Yoshida, S., et al. 1997. Involvement of interleukin-8, vascular endothelial growth factor, and basic fibroblast growth factor in tumor necrosis factor alpha-dependent angiogenesis. *Mol. Cell. Biol.* **17**:4015–4023.
37. Leibovich, S.J., et al. 1987. Macrophage-induced angiogenesis is mediated by tumour necrosis factor-α. *Nature.* **329**:630–632.
38. Lin, E.Y., et al. 2006. Macrophages regulate the angiogenic switch in a mouse model of breast cancer. *Cancer Res.* **66**:11238–11246.
39. Nozawa, H., Chiu, C., and Hanahan, D. 2006. Infiltrating neutrophils mediate the initial angiogenic switch in a mouse model of multistage carcinogenesis. *Proc. Natl. Acad. Sci. U. S. A.* **103**:12493–12498.
40. Bernardini, G., et al. 2003. Analysis of the role of chemokines in angiogenesis. *J. Immunol. Methods.* **273**:83–101.
41. Kune, G.A., Kune, S., and Watson, L.F. 1988. Colorectal cancer risk, chronic illnesses, operations, and medications: case control results from